POSITRON SOURCE FOR ILC[1]
A PERSPECTIVE

Alexander Mikhailichenko, LEPP, Ithaca, NY 14853

Abstract. Parameters of positron source specified to meet the requirements of BCD. The positron source includes the helical undulator, target for gammas, collection optics and the collimation system.

At the first stage unpolarized positrons in the quantities required can be generated with relatively short, ~20 m long, but strong (K~1) undulator. An undulator with the length increased to ~150 m and reduced K~0.4 can produce positrons with a polarization of ~75%. With a 250 m–long undulator polarization can reach ~85%. Recent developments show that the positron wing of the linear collider can operate independently from the electron one. Other advantages of positron production with an undulator are associated with much less radioactivity and relaxed conditions for the target. *Polarized electrons can be generated in this way as well.*

Described are our plans/visions for the development of such a system based on many-years- activity on this field since its invention in 1979.

INTRODUCTION[2]

High energy electron–positron collisions are essential for understanding the fundamental properties of matter. In pursuit of this understanding, the world physics community has put the International Linear Collider (ILC) project forward as the next instrument of choice. Although the basic idea of such collider is rather simple, the technology is challenging. One of the challenges is the production of positrons sufficient for the required luminosity. A new approach that is not possible at the energies of previous e^+e^- colliders has been adopted for the Baseline Concept Design (BCD) and involves a short period helical undulator as its essential component.

In this approach, electrons/positrons of the main beam, passing through the undulator, generate circularly polarized photons. These photons are further used for conversion into positrons in a thin target. The scheme of positron production with gammas, obtained from the helical undulator is represented in Fig.1[3].

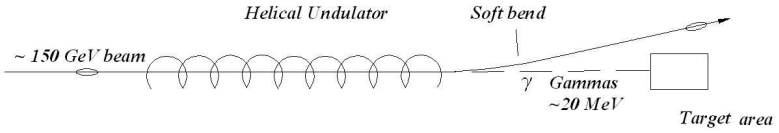

Figure 1: General scheme of conversion system.

Shown here are high energy electrons (or positrons) after reaching ~150 GeV in linear collider

---

[1] This is an extended version of a Talk represented at Snowmass 2005, http://www-conf.slac.stanford.edu/snowmass05/proceedings/proc/papers/ILCAW0313.PDF
Electronic version is available at http://www.lns.cornell.edu/public/CBN/2006/CBN06-1/CBN06-1.pdf.

[2] For review of positron production for Linear Collider see: a) A. Mikhailichenko, "*Polarized Positron Sources*", Workshop on e+e- Sources and Pre-accelerators for Linear Colliders, Schwerin, Germany 1994, Proceedings, pp. 61-75. b) A. Mikhailichenko, "*Use of undulators at high energy to produce polarized positrons and electrons*", published in the Proceedings, Edited by J. Clendenin, R. Nixon. (SLAC-R-502), pp. 229-289, a Talk given at Workshop on New Kinds of Positron Sources for Linear Colliders, Stanford, CA, 4-7 Mar 1997.

[3] V.E.Balakin, A.A.Mikhailichenko, "*Conversion System for Obtaining Highly Polarized Electrons and Positrons at High Energy*", Budker INP 79-85, September 13, 1979.

going through the undulator and then return to the main linac for further acceleration and collision at the IP. Gammas radiated in the undulator are directed to a thin (~0.5X_0, i.e. half radiation length) target. Positrons from electron-positron pairs are collected by short focusing lens, accelerated in the "pre-accelerator" and directed to a damping ring for further cooling. This method has been tested recently[4] and demonstrated polarized positron production in quantities as predicted. Production of circularly polarized gammas by wiggling of energetic (~150 GeV) electrons/positrons in static field of helical undulator looks much simpler, that the one associated with wiggling of low energy beam (~5GeV) in helical field of laser radiation.

General view of ILC with undulator is represented in Fig.2[5].

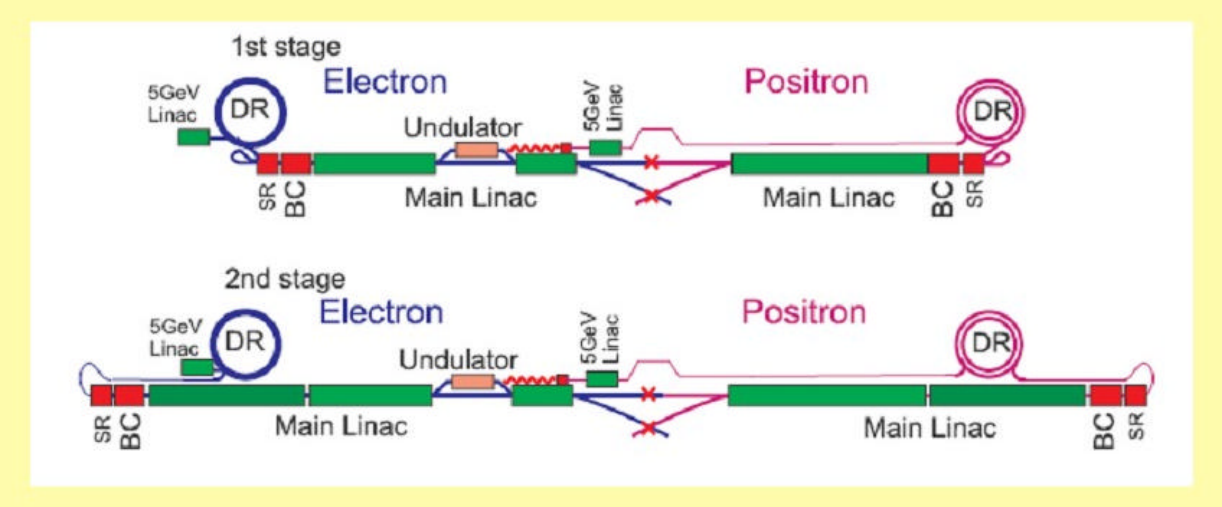

Figure 2: Schematic overview of Undulator Based Positron Source in which the helical undulator is located at the 150GeV point in the electron main linac. The undulator located in chicane shifted from the linac axis ~1m. Here the schemes for positron production by electrons are represented. It is possible to arrange self reproduction of positrons as well, see below.

For a 1 TeV upgrade of linear collider supposed, the undulator remains in the same position. In this case we recommend the period of the undulator to be slightly longer, 12 mm, to accommodate for this energy increase in the future. We plan to test both 10 and 12 mm periods, however.

BCD suggested the ~round ring as a baseline, however keeping dog bone-type cooler as an option. Each of these schemes has some advantages, undulator location and configuration is not affected by this at all. Usage of two damping rings for positrons makes problem of timing much easier. While in the second (final) ring the beam is cooled and prepared for injection into linac, the portion of positrons arriving from the other wing of linac is stored temporary in the first ring, having wider dynamic aperture on expense of higher equilibrium emittance.

To work at lower energy, (Giga-Z), the 150 *GeV*-beam, after passing the undulator decelerated in residual part of the accelerator. As the energy spread generated in the undulator, is increased, during deceleration some losses of luminosity is possible. The undulator parameters in this

[4] A. MIkhalichenko, "E-166 Status", a Talk at Snowmass 2005, http://www-conf.slac.stanford.edu/snowmass05/proceedings/proc/pres/ILCAW0313_TALK.PDF

[5] B.Barish, ATalk at ILC GDE Meeting at LCWS 06, 9 March 2006.

regime of operation can be optimized, so the luminosity reduction is minimal. It was shown that this is the best strategy for the emittance conservation[6].

Debuncher before damping ring required to control the length of the bunch before injection. Gamma beam has the same time/length structure as beam in main linac, where the length of the bunch is ~0.3mm. The lengthening defined by different path lengths in collection optics and by energy spread of collecting particles. Short bunch might trigger the instabilities in a damping ring. Equilibrium bunch length in a damping ring (~6 mm) is much longer, than in linac (~0.3mm); remember two-stage buncher at the linac entrance). Bends to the main linac and return loops for TESLA type cooler can be located in the same tunnel, Fig.3 upper picture. More detailed view on undulator chicane is represented in Fig.4.

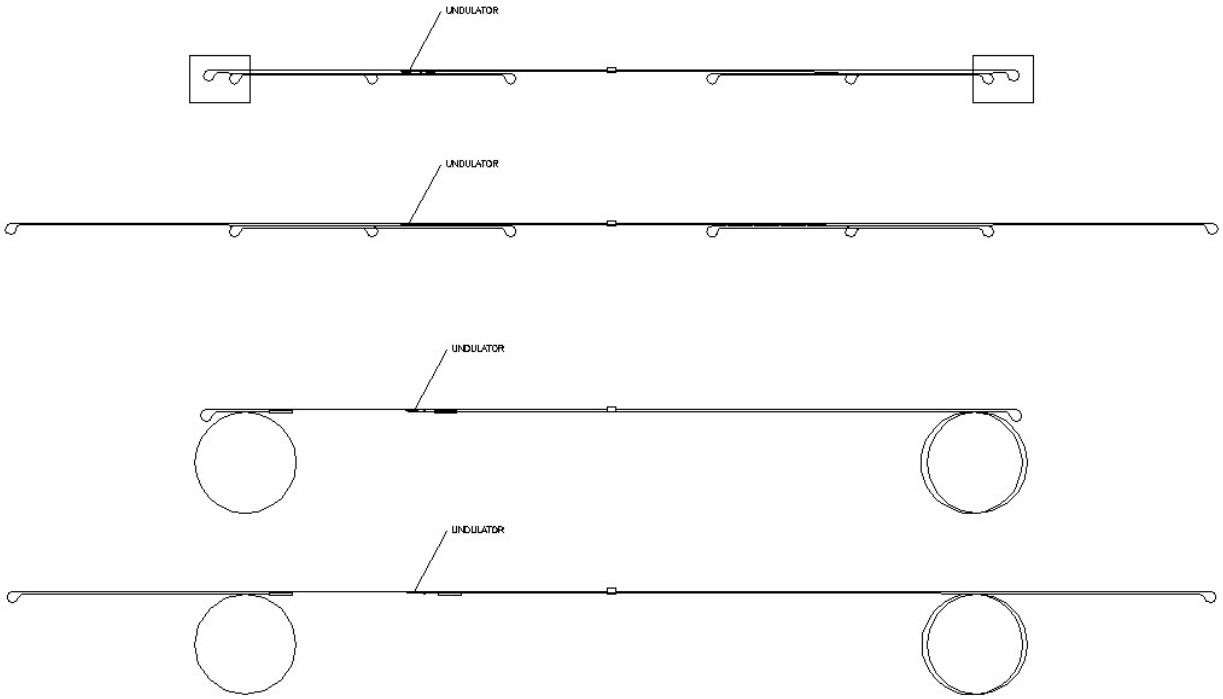

Figure 3: Scaled layouts of ILC with TESLA dog bone-type cooler for 500 GeV and 1TeV cm energy, two upper pictures. The scheme with round ring having diameter ~2km, two lower pictures. TESLA type cooler can have perimeter 6km or 12 km depending on progress in kicker and electron cloud instability in positron ring (shape remains the same, however).

Bending the beam off axis of the linac and back (chicane) is done with the help of achromatic bending system originated long time ago[7]. The parameters of this chicane are pretty straightforward. SR from bending magnets was found to be acceptable. Envelope functions are similar to what represented in Fig. 7. The off axis distance ≤ 1 m required just bypass the accelerating structures of pre-accelerator or accelerating structures of keep alive source if it is located on the line of main accelerator parallel to undulator. As undulator itself has ~120 mm outer diameter, this number gives the limit from it lower side. At this chicane some diagnostics can be provided. These may include measurements of polarization, beam emittance and so on.

[6] K.Kubo, " Effect of Transverse Wakefield in Low Energy Operation (Giga-Z)", 200508xx.

[7] V.V. Vladimirsky, D.G. Koshkarev, "*The Achromatic Bending Magnet System*", Instr. Exp. Tech.(USSR), (English translate) N6, 770(1958).

Target area located just behind the bending magnet. As at this location the linac is omitted, there will be no problem in positioning the target, collection optics and first RF post capturing sections.

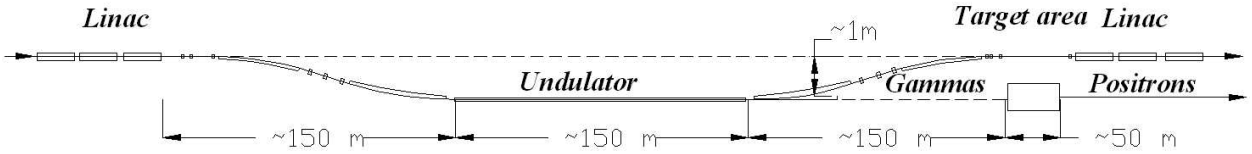

Figure 4: Scaled view of the space around undulator. Transverse scale enlarged.

So the total longitudinal distance occupied by conversion system (without 5 GeV post-accelerator) is ~500m.

Let us remind the basic parameters of positron conversion system as they are represented in BCD.

Number of particles per bunch	$N_b = 2\times10^{10}$
Number of bunches per train	n_b=2820 (5640)
Repetition rate	f=5 (10) Hz
Bunch sequence	~308 (154) ns
Total train duty	~1ms
Positrons–Target/IP	1.5
Undulator period	12 (10) mm
Undulator length	20-200 m
Undulator strength	1-0.4

We would like to underline, that those parameters of undulator scheme indicated in BCD as 200m and K=1 are not required at the same time. For 150 m long undulator and for single target, the field strength required for K~0.4 only (for two target scheme these numbers are even less, see lower).

As far as focusing along the undulator, it is not required in general. Envelop function of the order of the undulator length, ~200m is acceptable. However there is a desire to have the transverse beam sizes in undulator and on the target to be the same. So some optics can be introduced as the quadrupole lenses. As the undulator is sectioned this is not a problem at all.

So we are paying attention to all elements: undulator, target, collection optics, collimators and preliminary acceleration right after the target. Spin manipulation, injection optics down to damping ring and scheme of stabilization of current are another points of interest.

This scheme is also working for polarized electrons production.

COMBINING SCHEME[8]

Attenuation coefficient for the photons passed through the target is $k \approx \exp(-\frac{1}{3}\frac{7}{9}t)$, where t is the thickness of the target measured in units of X_0 (see (6)). For $t \approx 0.5$ (i.e. half radiation length)

[8] A.A. Mikhailichenko, *"Conversion System for Obtaining Polarized Electrons and Positrons at High Energy"*, Dissretation, Novosibirsk 1986, Translation in CBN 02/13, Cornell, 2002.

coefficient is around 0.87 i.e. only 13% of photons interact in a target. So it is possible to install second target and collect positrons independently from this second target. Combining could be arranged easily in the same separatrix of damping ring RF. Additional feedback system will be required for fast dump of coherent motion. This scheme represented in Fig. 4.

Here the gammas from the undulator are coming from the left side and illuminate the target *T*. The short focusing lens *L* collects the particles and adjusts for further optics. Collimator *C*, located in front of accelerating structure cuts the particles with large transverse angle. By doing this it also cuts particles with low moments as this particles over-focused by lens *L*. An acceleration section A_1 delivers energy E_1 for the secondary beam. This beam of positrons is bending with the help of magnet M_1. The magnet M_1 and a part of the magnet M_3 with quadrupoles *l*, make an achromatic parallel shift of the positron beam. The second acceleration section A_2, delivers lower energy $-E_2$ to the beam, collected from the *second* target. The magnet M_2 with the part of the magnet M_3 and lenses, adjusted for achromatic parallel shift of the beam with the energy E_2. The difference in the path lengths of these two lines is an integer and a half of the wavelength in structure A_3. So the first sections in A_3 eliminate the energy difference. *D* is the gamma beam dump[9]. Structure A_4 is a pre accelerator which accelerates bunches to the energy required for delivering positron bunch to the location of main linac which finally rises energy up to injection one for the damping ring.

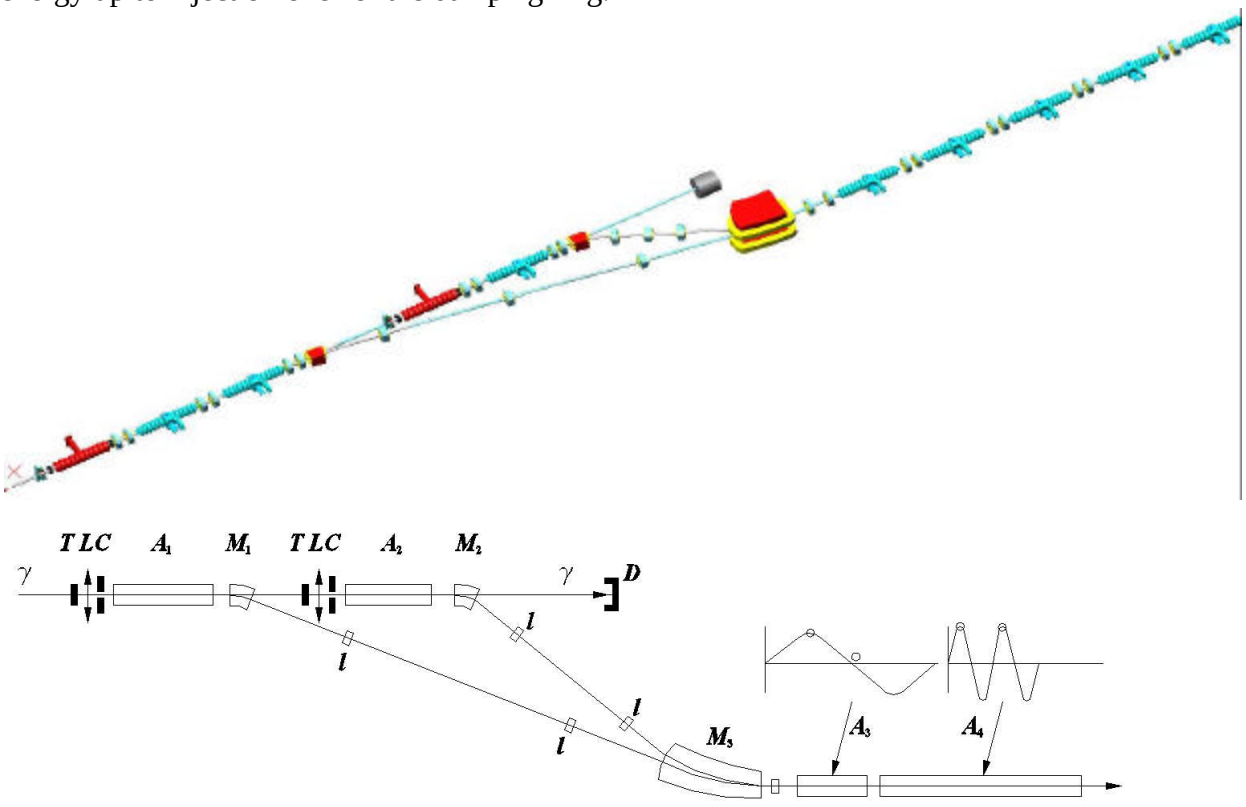

Figure 4: Combining scheme. Energy provided by acceleration structures $\boldsymbol{A}_1$ and $\boldsymbol{A}_2$ are slightly different, $\boldsymbol{A}_1 > \boldsymbol{A}_2$. T stands for target, ***L*** –is a short focusing collection lens, ***C***–is a collimator, ***l***–is a quadrupole lens, ***D***–is a gamma beam absorber.

[9] In simplest case the gamma-beam dump is the collimator with hole diameter → 0. It must be able to accept full power of gamma beam ~35 kW.

As the process of positron creation is axisymmetrical as well as short focusing optics is axisymmetrical too, the combining can be arranged in vertical plane for fitting in the tunnel. In this case all magnets: M_1, M_2, M_3 bend in vertical direction. Any arbitrary angle is allowed as well.

Suggested average energy for the first structure A_1 is E_1=215 ± 5 *MeV* and for the second structure E_2 =175 ± 5*MeV*.

After energy is equalized two bunches can be stacked in the same separatrix. Feedback dumps coherent motion of centroids.

This combining can help in reduction of power deposition in target if each target made thinner, than optimal.

INDEPENDENT OPERATION OF ELECTRON/POSITRON WINGS

More detailed scheme of positron source is represented in Figure 5. Here we took the scheme with TESLA type ring. Thanks to the presence of starter source, the positron wing of collider works independently from the electron one[10]. Starter source (having the size of a barrel) generates low intensity, 1 MeV electrons which are accelerated in the main structure up to 0.5 GeV[11]. *Electrons* directed then to the positron target, the same as for polarized positron production, where they are generating positrons, which are collected by the same optics. After the necessary amount is accumulated (stacked) in the damping ring, the beam from damping ring goes into main linac. After few cycles, the polarized positron beam becomes restored. Soft bend off acceleration line to the undulator axis made achromatic. Feedback system, operating on bunch to bunch basis, makes this scheme stable under charge fluctuation. Starter linac located on the lane of main linac in the region where the undulator is located. Starter source plus following linac, delivering 0.5 GeV is what *we* call "keep alive source".

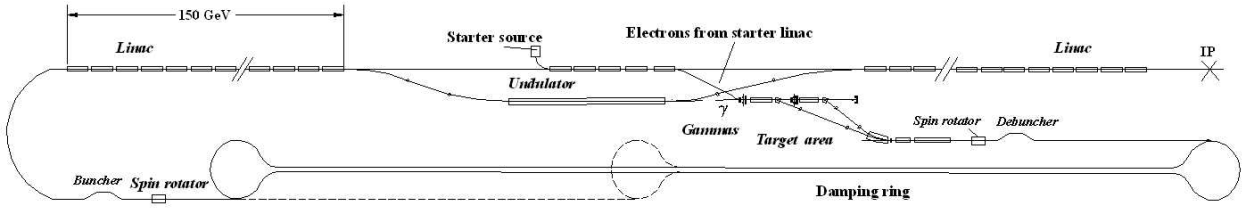

Figure 5: Positron wing of collider works independently from electron one, thanks to the presence of starter source. Here we represented the scheme with TESLA type ring

Namely, let us scale the view of target area in Fig.5[12]. Let us consider the one line only.

[10] A. Mikhailichenko, "Why polarized positrons should be in the base line of linear collider", CLNS 04/1894, November 24, 2004.

[11] This can be combined with main linac for the lowering of cost.

[12] A. Mikhailichenko, "*Fast Bunch to Bunch Intensity Regulation in the ILC Conversion Scheme with Independent Electron/Positron Sections*", CBN 05-18, August 14, 2005 . http://www.lns.cornell.edu/public/CBN/2005/CBN05-18/CBN05-18.pdf

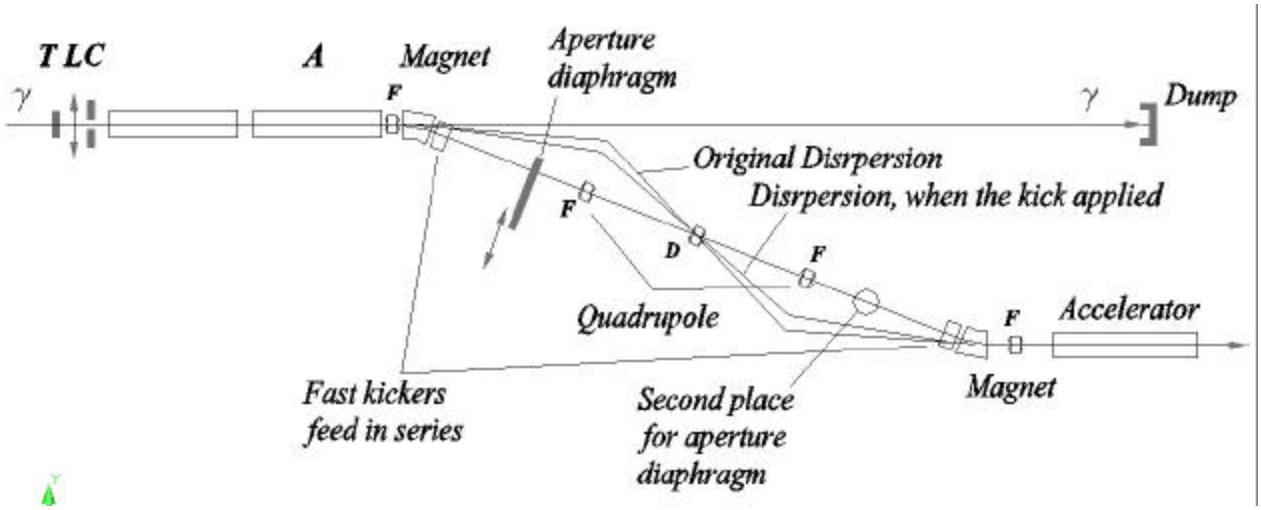

Figure 6: Achromatic bend with aperture diaphragm. *T*–is a target, *L*–is a short focusing lens, *C*–stands for collimator. *F* and *D* stand for focusing and defocusing lenses respectively. *A* stands for the RF accelerator structure.

For stable operation of the loop, self regenerating positrons, special fast feedback which includes pair of fast kickers (Fig.6), aperture diaphragm and system for bunch to bunch population measurements required. As the each bunch reproduces itself, so the bunch population measured in a damping ring. To the moment of collection of positrons regenerated through gamma-beam, feedback system gives controllable kick, so the collection efficiency for this particular bunch is changed by combination of kicker/diaphragm[11].

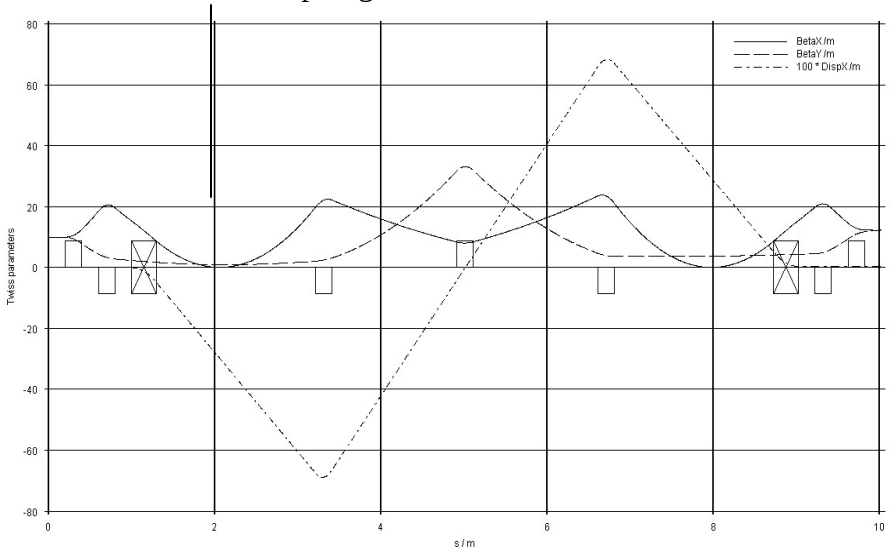

Figure 7: Example of a more detailed design of channel for parallel beam shift. Envelope functions and dispersion are given in meters. Scraper location indicated by arrow. Radial beta-function in minimum is ~4 cm.

THE POWER BALANCE IN GAMMA BEAM

First of all one can see that *intensity of radiation* in the helical undulator is two times higher, than in planar undulator with the same period and *K* factor. This is because in helical undulator particle participates in acceleration in two geometrical planes, (vertical and horizontal) while the acceleration in planar undulator is going in one direction only. As the radiated field with every polarization is proportional to acceleration in the corresponding direction, this yields the intensity balance just mentioned. Spectral density of radiation is two times higher also. Numerically

$$\left.\frac{dI}{dx}\right|_{helical} = 2\left.\frac{dI}{dx}\right|_{planar}, \qquad (1)$$

where $x = \frac{\hbar w_g}{\hbar w_{g\,\max}}$ is a ratio of current photon energy to the maximal possible one at first harmonic. From the formula for radiation

$$\frac{dN_g^{helical}}{dx} = \left.\frac{dI}{dx}\right|_{helical} \cdot \frac{1}{\hbar w^{helical}} = \sum_n \frac{dN_{gn}}{dx} \approx 4\pi\alpha M \frac{K^2}{1+K^2} \sum_n nF_n(K,x), \qquad (2)$$

where *M* stands for the number of periods and *n* stands for harmonic number, $M = L / l_u$, $\alpha = e^2/\hbar c$ –is a fine structure constant. Functions

$$F_1(K,x) \cong \tfrac{1}{2}(1-2x+2x^2), \quad F_2(K,x) \cong 2x(1-x)(1-x+2x^2)K^2. \qquad (3)$$

Integrating over x one can obtain *the number of radiated photons* for the first harmonic

$$N_g^{helical} \approx \int_0^1 \frac{dN_g^{helical}}{dx} dx \approx 4\pi\alpha M \times \frac{1}{6} \times \frac{K^2}{1+K^2} \qquad (4)$$

The total number of photons in all spectrum radiated in undulator having *M* periods and undulatority factor *K* goes to be

$$N_g \cong \frac{4\pi}{3}\alpha \cdot M \cdot \frac{K^2}{1+K^2}$$

For 100 m-long undulator with period $l \cong 1$ cm, $M=10^4$. For $K^2=0.15$ the last formula gives $N_g \cong 80$ photons. As the energy of each photon for primary beam energy $E \cong 150 GeV$ goes to be

$$E_{g\,\max}[MeV] \cong \frac{2.48 \cdot (\gamma/10^5)^2}{l_u[cm](1+K^2)} \cong \frac{2.48 \cdot 9}{1.15} \cong 19.4,$$

then the total number of photons per bunch goes to be $N_{g\,bunch} \cong 80 \times 2 \cdot 10^{10} = 1.6 \cdot 10^{12}$ and the total energy carried by all the photons radiated by bunch goes to be

$$E_{g\,bunch} \cong N_{g\,bunch} \times E_{g\,\max} \cong \tfrac{1}{2} \times 1.6 \cdot 10^{12} \times 19.4 \cdot 10^6 \times 1.602 \cdot 10^{-19} \cong \tfrac{1}{2} \times 1.74 \times 1.94 \times 1.6 = 2.5\ [J].$$

where factor ½ takes into account that the half of the photons carry this energy. Train will radiate

$$E_{g\ train} @ N_{g\ bunch} \times E_{g\ \max} \times n_b @ E_{g\ bunch} \times n_b = 2.5 \times 2820 = 7644\ [J] \cong 7kJ,$$

and the energy carried by all photons radiated per second will be $E_{g\ tot} \cong 35kJ$. The power carried by these photons goes to be $P \cong 35\ kW$. For 20 MeV gammas approximately 13% of gammas deposited theirs energy in the target, brining the power deposited in the target to $P_{target} \cong 4.55$ kW.

So the average energy deposited in the target is not high, but the pulsed energy deposition makes the target problem severe, however.

UNDULATOR

Undulator is a key element in this scheme. Activity in Cornell is covering the modeling of fringe fields, fabrication and test of prototypes and modeling technology. Aperture clean for the beam will be 8mm[13]. Vacuum chamber made from Oxygen-free Copper. Perturbation of emittance in undulator is a key issue and calculations are rechecked. Simulation of different entrance tapering is under progress. Restoration of "start to finish" simulation code is under progress. It was written for Li lens as a focusing element now it is added to Solenoidal focusing.

Fringe fields compensation. This is the mostly important item for the scheme, as the undulator installed before IP. Methods of compensation include proper tapering and installation the sections in series with alternative polarities. Tiny vertical emittance puts the limit for the field imperfections.

Test of module with beam at low energy can be done at Cornell. Some other Laboratories have abilities for such a test as well.

Perturbation of emittance is a crucial moment of all method, if undulator installed before IP. (See Appendix). 2 m—long sections with the same spatial orientation of input and output ends installed in series and feed with opposite polarity. This automatically delivers first integral

$$I^1_{x,y} = \int_{-\infty}^{+\infty} H_{x,y}(s)ds = 0.$$

This integral is responsible for transverse kick, as $x' = I^1_x/(HR)$, $y' = I^1_y/(HR)$. So the 4m—long module delivers zero kick. To eliminate displacement, two 4 m-long modules need to be fed with opposite polarity. This will bring second integral to zero $I^{(2)}_{x,y} = \int_{-\infty}^{+\infty} ds \int_{-\infty}^{o} H_{x,y}(s)ds$ So two 4 m –long sections deliver zero first and second integral.

Undulator under design done at Cornell, implements the Oxygen-free Copper (OFC) chamber having an inner diameter of 8mm. So the vacuum is not a problem here. Resistive wall instability in Copper chamber is cooled to LHe temperature for the beam moving in vacuum chamber was considered and no problems were found here.[14]

---

[13] We would like to attract attention that this aperture is bigger, than suggested for LCLS (6mm). Our technology allows much higher field and bigger aperture, than in planar PM undulator accepted as a base line for LCLS. Implementation of our technology allows drastic reduction of the length and cost of LCLS.

[14] A.A. Mikhailichenko, V.V. Parkhomchuk, *"Transverse Resistive Instability of a single Bunch in a Linear Collider"*, Preprint INP 91-55, Novosibirsk, 1991.

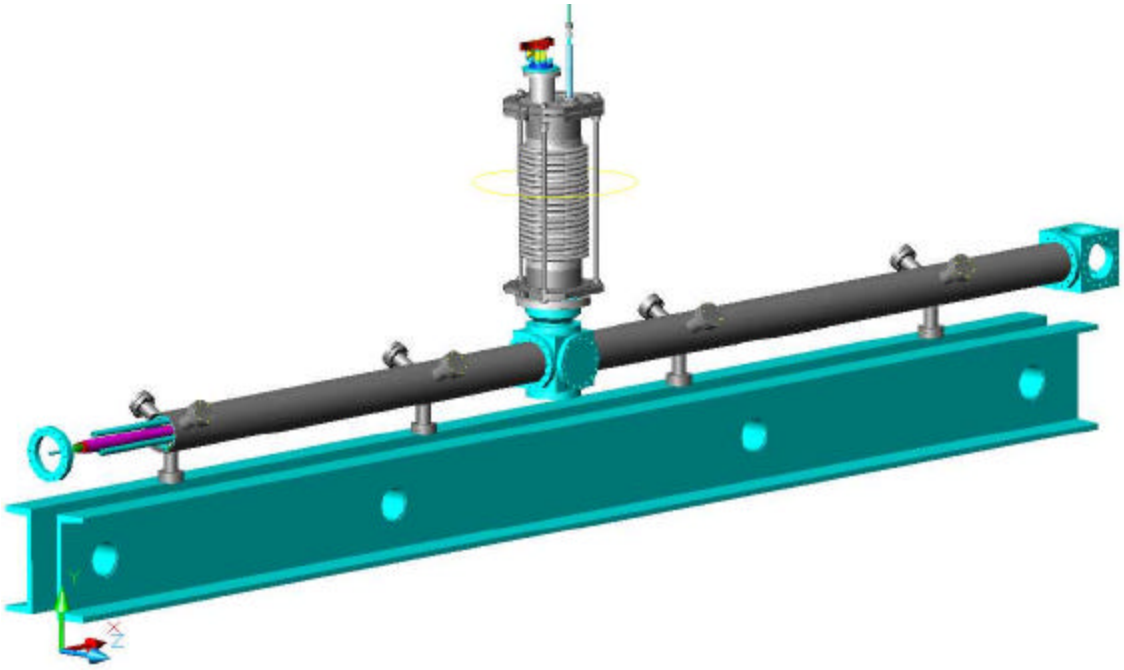

Figure 8: Cryomodule, 4 m—long. Cryostat contains two 2 m–long identical sections having opposite polarity. This delivers zero first integral along this module. Some part of vacuum chamber removed for better inside visibility.

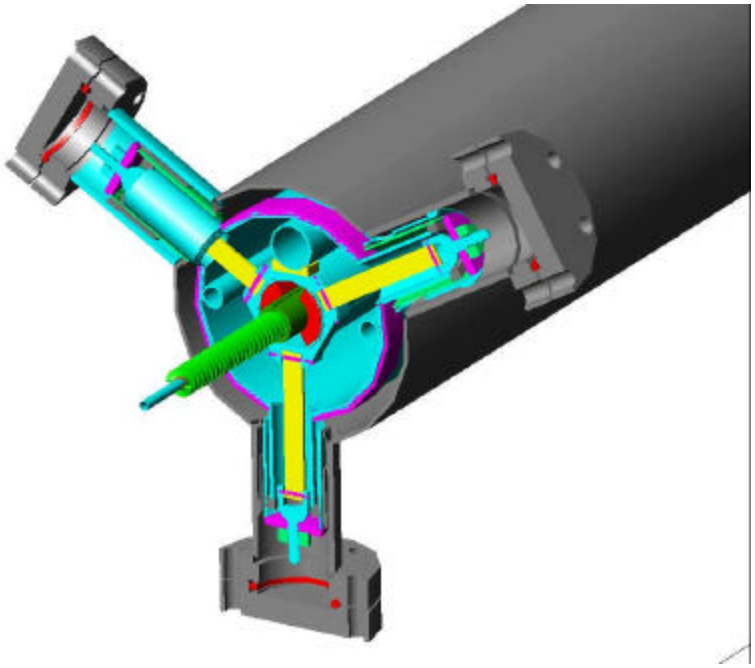

Figure 9: Details of cold mass support. Outer tube diameter is 5 inch.

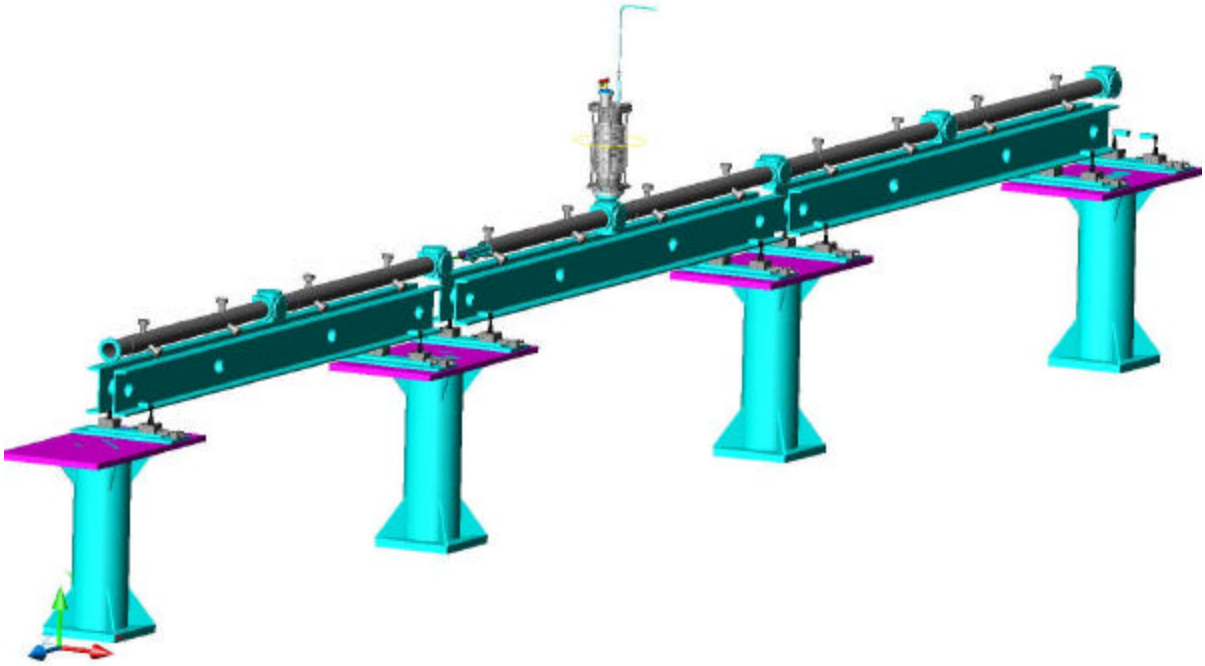

Figure 10: Sections installed in series.

Strategy for tuning and alignment.

Correction elements include trim coils allowing generating dipole field in two rectangular directions located at the ends of each module. Natural realization of these trim magnets as having superconducting wiring and integrating into cryo-system.

Lower-impedance pickups are two types: one is a differential type located in short cavity covered by thin stainless steel foil and the second one located *outside* of perforated tube serve as a continuation of vacuum chamber in joint . These perforations made for the purposes of vacuum pumping.

We are considering few scenarios for tuning the undulator during installation. In one scenario the operation begins with ballistic passage of beam through un-powered undulator. During this passage the beam positions at pickup stations collected and processed. Then undulator is powered on and the trajectory measured again. On the basis of these measurements the commands are given to specific correctors to adjust the trajectory. Sections of undulator will be adjusted in positions with the help of remote movers with moderated resolution. Correctors are realized as additional windings in quadrupoles. Panofsky-Hand type of lens looks mostly suitable for these purposes. This allows avoid organizing mechanical movement of lenses.

COLLECTION OPTICS

We suggest a DC collection optics for ILC. In part, the collection optics of this type was under the test at E-166[15], where the short period focusing lens was a part of positron collection optics. Here the lens served as a quarter wave transformer (QWT). This lens allowed

[15] G. Alexander *et al.,"Undulator-based production of polarized positrons: A Proposal for the 50-GeV beam in the FFTB",* SLAC-TN-04-018, SLAC-PROPOSAL-E-166, Jun 2003. 67pp.

enhancement, defined as positron collected with lens on/off, of the factor of 8-10, depending on central energy. Focal distance of solenoidal lens is

$$F = \frac{4 \cdot (HR)^2}{\int H^2 ds} \tag{5}$$

For estimations, 10 MeV positrons /electrons have

$$(HR) = pc / 300 = \frac{10 \cdot 10^6}{300}[G \cdot cm] = \frac{10 \cdot 10^3}{300}[kG \cdot cm] \cong 33 kG \cdot cm$$

so for longitudinal axis field ~20 kG and continuity 3cm,

$$F = \frac{4 \cdot (HR)^2}{\int H^2 ds} = \frac{4 \cdot 33 \cdot 33}{20 \cdot 20 \cdot 3} \cong 3cm$$

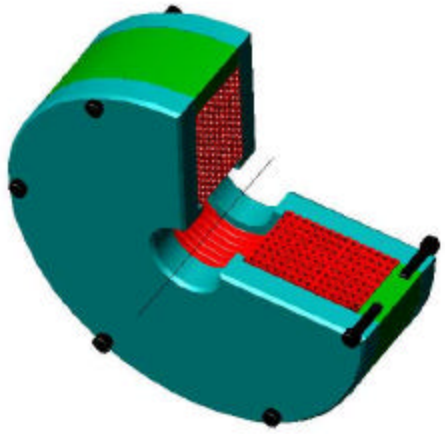

Figure 12: Cross section of E-166 short focusing lens.

This is a multi–turn lens wound with hollow copper conductor having rectangular cross–section. Current density reaches ~45 A/mm^2.

This lens can be considered as a prototype for the ILC one. Quasi—stationary feeding allows increase current up to 100 A/mm^2. This is possible taking into account that ILC beam lasts for ~1ms and repetition rate is only 5 Hz. So this lens can be fed with~ 5ms top flat current, arranged with the help of third harmonics. Thyristors can be used adequately here. Some parts of the yoke can be made with laminations. *So this type of lens solves the problem in principle*.

More fundamental solution is a SC lens.

For this lens we investigated iron-free solenoidal lens. The role of Iron important at lower field, however. Absence of iron allows reduction of the energy deposition by particles scattered from target. All vacuum chamber and cold mass container made from Al for reduction of isotopes accumulation.

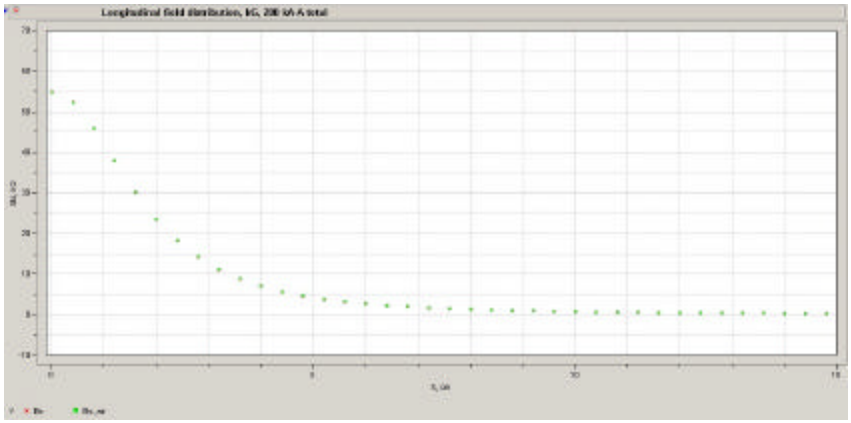

Figure 13: Field along axis with/without Iron yoke. Input from iron is small at this field level (50kG).

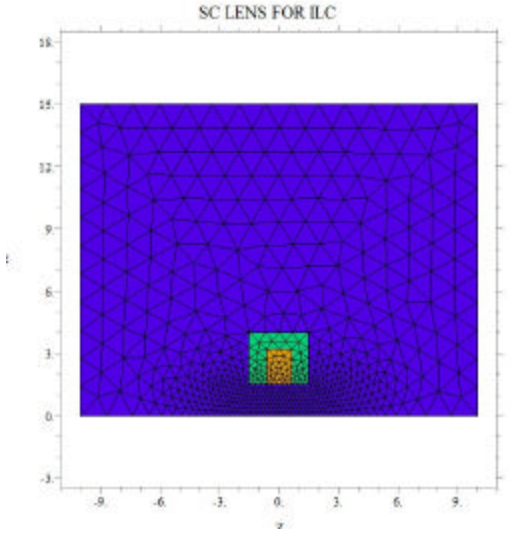

Figure 14: The mesh used for calculations.

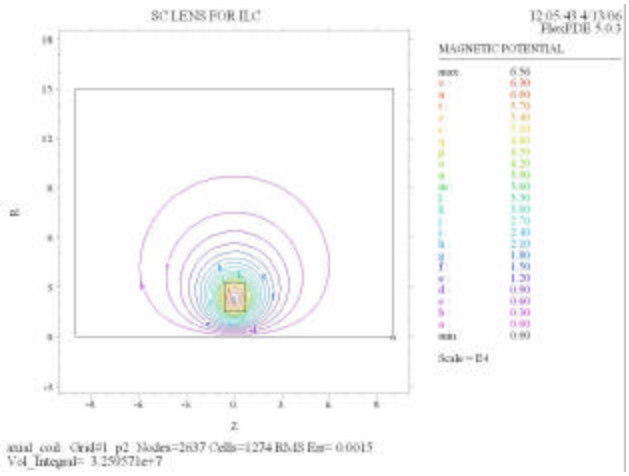

Figure 15: Field lines around SC lens.

The power carried by secondary positrons/electrons scattered in the target with big angles is of the order of 100W (of 35 kW). So the Tungsten disc located right behind the target having thickness ~20 mm intercepts practically all power remaining ~0.5-1W which can be handled by cooling system.

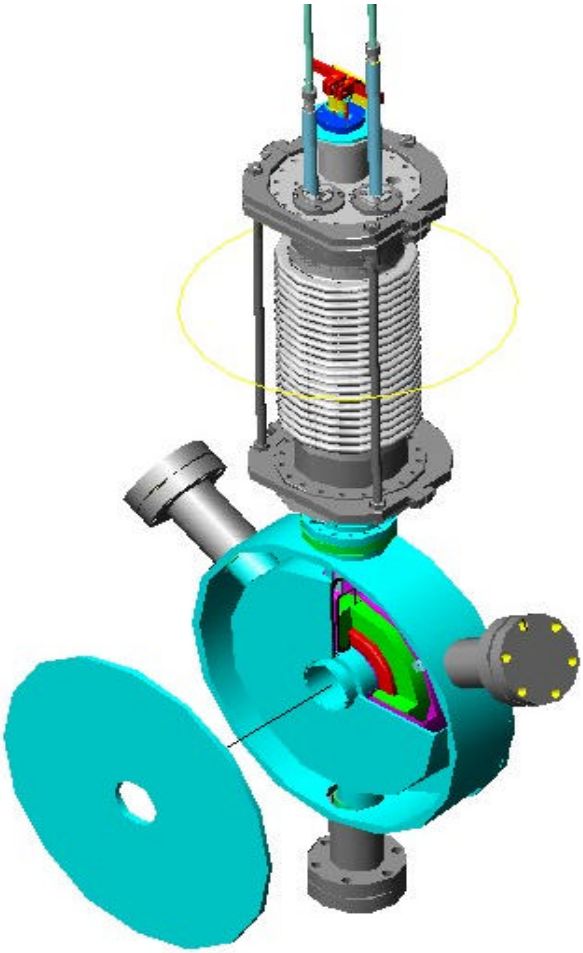

Figure 16: SC solenoidal lens.

So from the point of engineering this is pretty moderate device.

TARGET

Now the baseline for the target is a Titanium target wheel having diameter ~1m, 1.42 cm thick, rotating at 500 rpm[16]. Some questions remain however, namely if the target wheel immersed into magnetic field, what additional power required to rotate it and what is additional heating? In case if pulsed-collection optics in use, what might be impact of pulsed field to the fast moving wheel? What the fatigue damage of Ti wheel might be? Possibly, all these questions can be answered positively. We are looking for more guarantied schemes, however. One can find that investigations in this field are pretty actual due to requirements of muon collider project, see[17].

Shape of target. First, we investigated the targets of different shapes[18].

[16] J.Sheppard," RDR Status e+ Source ", e+e- Sources System Area Status Meeting, April 11, 2006, http://ilcagenda.cern.ch/getFile.py/access?resId=1&materialId=0&confId=309

[17] High-Power Targetry for Future Accelerators, Long Island, NY, September 8-12, in series of Workshops for muon collider: http://www.cap.bnl.gov/mumu/collab/table_workshop.html

[18] A.D. Bukin, A.A. Mikhailichenko, *Optimized Target strategy for Polarized Electrons/Positrons production for Linear Collider*, Budker INP 92-76, Novosibirsk, 1992.
http://www-project.slac.stanford.edu/lc/local/systems/Injector/Talks%20and%20Papers/PolPositronPapers/BukinandMikhaili9276.pdf

Short target | Longer target | Very long target | Very long target, front view

Figure 17: Different types of arrays of out-coordinate for positrons escaping from the target rod. For the very long target, most of the particles escape through the sidewalls. Lengths of the cylinders are not to scale with theirs diameter.

Calculation of capturing efficiency is done with numerical code CONVER and by trajectory tracking.

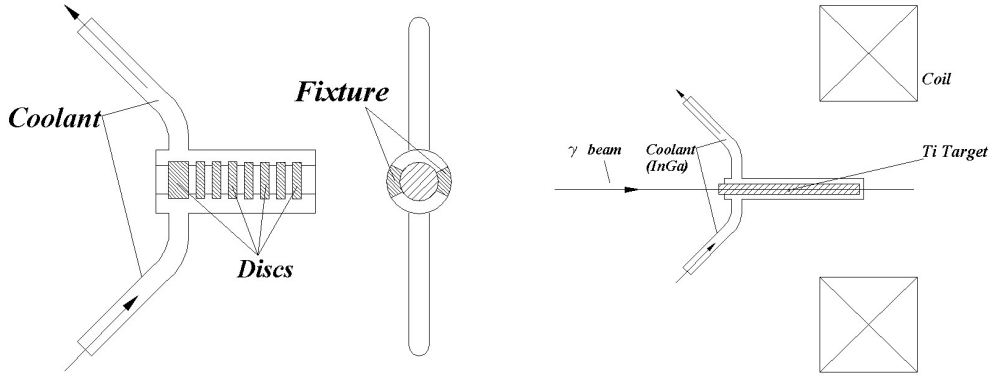

Figure 18: Sandwich-type high power target. W or Ti discs enclosed in Ti container with InGa coolant. At the right-long Ti target cooled by InGa coolant[1].

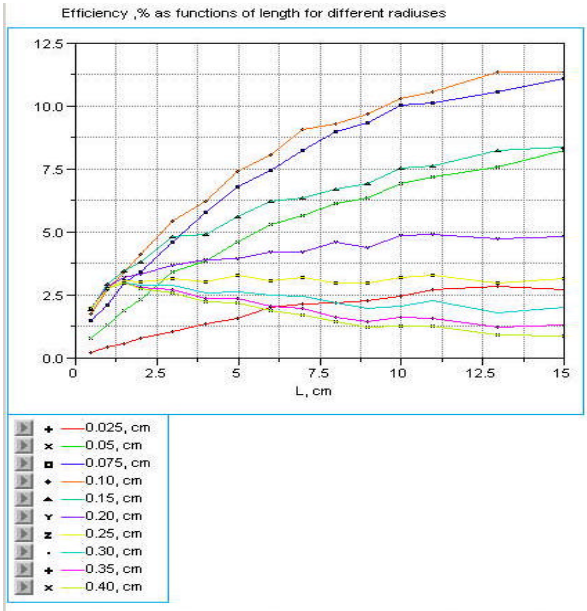

Figure 19: Efficiency as functions of target length for different values of radius.

Utilization of few targets, considered above and combining positrons into longitudinal phase–space is also some kind target-shape problem. One can decrease the thickness of the target and reduce the heating by this way.

In principle the needle type Titanium target has maximal yield. In addition to this option, we are considering some other possibilities for the targets.

One of these is a *liquid metal target*. Liquid metal targets have been considered earlier[8,19]. Here we represent our latest design for such system[1].

Liquid metal target

High Z metals could be used here are the Lead[20] (Pb), Bismuth-Lead (Bi-Pb) eutectic alloy, Mercury and even Wood's metal. *In-Ga alloy filled with W powder can be used as a target also.*

Mostly effective material from point of efficiency is Bi-Pb alloy, as all these elements have highest atomic number Z (^{83}Bi—^{82}Pb). Cross-section of positron production is proportional to $\sim Z^2$ (per nuclei). Bi-Pb alloy composed with 55.51Mass% of Bi and 44.49 Mass% of Pb has liquid phase at 125.9 ^{o}C. Phase diagram of this alloy is rather branchy with different modifications of Pb sub-phases. At 200 ^{o}C this eutectic has liquid phase for wide percentage of mass ratio. This alloy is broadly in use as a coolant for transportable Nuclear Power Installations. It is also in use as a target at SINQ[21]. We would like to mention here, that these elements (Pb and Bi) have lot of isotopes, numbered by few tens, which have broad rage of lifetimes. *Anyway Bi-Pb as a coolant is very suitable for positron production and can be considered as main candidate for this purpose*.

Effective radiation length calculated as

$$\frac{1}{X_{eff}[g/cm^2]} \cong \frac{\%Bi_W}{X_{Bi}} + \frac{\%Pb}{X_{Pb}} \cong \frac{0.555}{6.2} + \frac{0.445}{6.4} \cong \frac{1}{6.28}, \qquad (6)$$

which corresponds to geometric length $\cong X_{eff} / r_{eff} \cong 0.6cm$.

Liquid metal jet chamber (see Fig.20) designed so it can work with temperatures up to 450 ^{o}C, so it can accommodate even pure liquid Pb. One peculiarity here is that the liquid metal duct has profiled extension, so the overheated metal expands in this extension practically without developing pressure in the system. Thermal pressure p_T can be expressed as the following[22]

$$p_T = G(V)\frac{c_V T}{V} = G(V)\frac{e_T}{V}, \qquad (7)$$

where $G(V)$ characterizing the ratio of the thermal pressure to the specific thermal energy e_T / V called Grüneisen coefficient, c_v stands for the heat capacity. By introduction of thermal expansion coefficient

---

[19] a) V. Belov *et al.* "*Liquid metal target for NLC positron source*". SLAC-PUB-9418, PAC-2001-TPAH126, Aug 2002. 3pp. Presented at IEEE Particle Accelerator Conference (PAC2001), Chicago, Illinois, 18-22 Jun 2001.
b) G.I Silvestrov," *Liquid Metal Targets for Intensive High-Energy Physics Beams*", Workshop on New Kinds of Positron Sources for Linear Colliders, SLAC, Stanford, March 4-7. 1997, Proceedings, SLAC-R-502, p.367.

[20] P. Logachev, "*Liquid Metal Targets*", a Talk at Workshop on Positron Sources for the ILC, CCLRC Daresbury Lab, 11-16 April 2005, see http://www.astec.ac.uk/id_mag/PDF%27s/Positron%20Workshop%202005/Liquid%20lead%20target..pdf

[21] F.Groeschl, "*MEGAPIE-a Liquid Pb_Bi Target at SINQ*", Workshop on High Power Targetry for Future Accelerators, Ronkonkoma, 8.-12. Sept., 2003, see ref 16.

[22] Ya.B.Zeldovich, Yu.P.Raizer," *Physics of Shock Waves and High-Temperature Hydrodynamic Phenomena*", Vol.II, Academic Press Inc.1967, p. 697.

$$a = -\frac{1}{r}\left(\frac{\partial r}{\partial T}\right)_P = \frac{1}{V}\left(\frac{\partial V}{\partial T}\right)_P = \frac{1}{K_T}\left(\frac{\partial P}{\partial T}\right)_V = \frac{G(V)c_V}{K_T V} = \frac{G(V)c_P}{K_S V}, \tag{8}$$

where K_T is the isothermal bulk modulus, Grüneisen coefficient can be expressed as

$$G(V) = \frac{VaK_T}{c_v} = \frac{VaK_S}{c_P}, \tag{9}$$

where K_S is the adiabatic bulk modulus. Energy deposited in the volume defined by the gamma beam size at the target

$$p\sigma_{\gamma}^2 \approx p\sigma_{\gamma u}^2 + \frac{(ge)b}{\gamma} \approx pL\left[\frac{1+K^2}{\gamma^2} + \frac{(ge)}{\gamma b}\right] + \frac{(ge)b}{\gamma} \tag{10}$$

where (ge) stands for invariant beam emittance, b is envelope function in undulator, γ is a gamma factor of the beam and the term in brackets defines the input from the angular spread arisen from natural radiation spread $\sim 1/\gamma$, from the wiggling angle and from angular spread of the beam in undulator. Here we suggested that there is no focusing in undulator. By introduction of focusing and/or some steering of beam in undulator, one can artificially increase the gamma-spot size on the target. So the total volume is

$$V \approx p\sigma_{\gamma}^2 Ll_T \approx \frac{p}{2}\sigma_{\gamma}^2 Ll_{X_0}, \tag{11}$$

where $l_T \approx l_{X_0}$ is the thickness of the target. For consideration of target conditions during a single bunch pass, one can accept that the beam energy deposited in this volume instantly, linearly increasing to exit of target. The energy Q_{bunch} deposited by the bunch in the target is $Q \approx 0.15 - 0.2\ J$ depending on details of focusing in undulator. So the pressure existing at the very first moments comes to[23]

$$p_T = G(V)\frac{e_T}{V} \approx G(V)\frac{Q}{p\sigma_{\gamma}^2 l_T}\left[\frac{z}{l_T}\right], \tag{12}$$

where z coordinate runs from the entrance of target. As the Grüneisen coefficient for typical case ~1.5-2 then the thermal pressure at the first moment comes to *kbar* level.
Temperature dynamics in a target governed by equation

$$\nabla(k\nabla T) + \dot{Q} = rc_V\dot{T}, \tag{13}$$

where k stands for thermal conductivity, $\dot{Q}[Watts/cm^3]$ –density of energy deposition. In cylindrically symmetric case with isotropic thermal conductivity, this equation expands

$$\frac{\partial^2 T}{\partial r^2} + \frac{1}{r}\frac{\partial T}{\partial r} + \frac{\partial^2 T}{\partial z^2} + \frac{1}{k}\dot{Q}(r,z,t) = \frac{rc_V}{k}\frac{\partial T}{\partial t}. \tag{14}$$

The time scale of this equation defined by its characteristic equation (what introduces the thermal skin layer)

$$dr^2 \approx dt\left[k/rc_V\right]. \tag{15}$$

If we substitute here for the distance the one corresponding propagation of perturbation with a speed of sound, $dr \approx v_s t \approx v_s l_T / c$, then

[23] T.A. Vsevolojskaya, A.A.Mikhailichenko, E.A.Perevedintsev, G.I Silvestrov, A.N.Cherniakin, "*To the Project of Conversion System for Obtaining Polarized Beams at VLEPP Complex*", internal report BINP, Novosibirsk, 1986.

$$dt \approx \frac{v_s^2}{c^2} l_T^2 \frac{r c_V}{k}. \qquad (16)$$

Substitute here parameters of Hg (as example, see Table 1). One can obtain that this characteristic time of relaxation for this distance

$$dt \approx \frac{v_s^2}{c^2} l_T^2 \frac{r c_V}{k} = \frac{1.96 \times 10^6}{9 \times 10^{16}} (5 \times 10^{-3})^2 \frac{13.6 \times 10^3 0.14 \times 10^6}{8.34} = 1.3 \times 10^{-7}\ s,$$

is much longer, than the bunch pass-time $t \approx l_T / c \approx \frac{0.5}{3 \times 10^{10}} \approx 1.7 \times 10^{-11}$s. In this case it is possible to average equation (14) over bunch pass-time. In this case it comes to the form

$$\frac{\partial^2 \bar{T}}{\partial r^2} + \frac{1}{r}\frac{\partial \bar{T}}{\partial r} + \frac{\partial^2 \bar{T}}{\partial z^2} + \frac{1}{k} Q(r,z,t) = \frac{r c_V}{k}\frac{\partial \bar{T}}{\partial t}, \qquad (17)$$

where $\bar{T}(t) = \frac{1}{t}\int_t^{t+t} T dt = \frac{c}{l_T}\int_t^{t+t} T dt$ and c_V expressed here as a specific mass heat capacity. This procedure simplifies evaluation of term with density of energy deposition. Such average temperature has direct physical sense as an average over time interval. In this case the Power deposition can be evaluate as

$$Q(r,z,t) = \begin{cases} \dfrac{2Q_{bunch}}{p\, s_{\perp g}^2 l_T t} \times \dfrac{z}{l_T}, & t = 0 \\ 0, & t > 0 \end{cases}$$

In this case solution of (17) becomes a trivial problem. To confirm this we arranged numerical model using FlexPDE for equation (13) with the source

$$\dot{Q} = \sum_i \frac{2cQ_{bunch}}{p\sqrt{p}\, s_z s_{\perp g}^2 l_T} \frac{z}{l_T} \exp\left(-\frac{(z + z_0 - c(t - i \times t_0))^2}{s_z^2}\right) \times \exp\left(-\frac{r^2}{s_{\perp g}^2}\right), \qquad (18)$$

Q_{bunch} stands for the energy deposited by single bunch, i –numerates the bunch, z_0 initial displacement. Expression normalized so that for single bunch

$$\int_0^{\infty} dt \int_0^{Volume} \dot{Q}(r,z,t) dV = Q_{bunch}. \qquad (19)$$

Some results of this modeling are represented in Fig. 20 below.

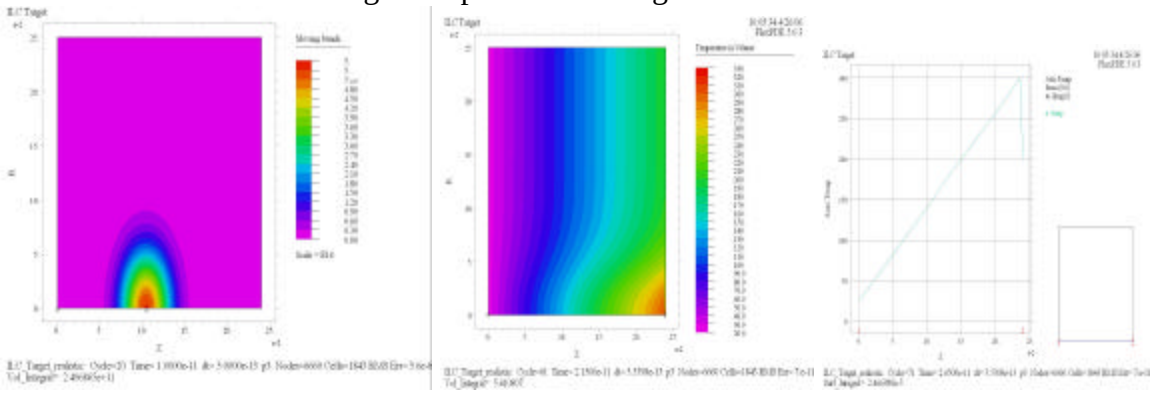

Figure 20: Left to right-The bunch moving in the target, Isotherms after the passage, temperature profile along the beam axis.

In this numerical model the flanges supported at different temperatures and the properties of Mercury were substituted here. This modeling, showing dynamics of heating indicate good agreement with analytical estimations.

For Bi-Pb alloy the one minor negative fact is it's operational temperature ~150 ^{o}C. Once again, operation of this alloy as a coolant in nuclear power plants is rather developed industry. Compared with technique in use in accelerator engineering it is not a problem to accommodate this technique. As we just mentioned our Liquid Metal Jet Chamber (LMJC) can work with such temperature without any problem. So the other elements of the counter such as gear pump, heat exchanger, filing and filtering systems can work under this temperature as well.

Other material for the target is Mercury (Hg). One peculiarity in usage of Hg is its low boiling temperature (~356^{o}C). That means, when the heat absorbed brings Hg to the boiling point the *latent heat of vaporization* comes on scene, which allows absorbing significant amount of heat energy having moderate temperature. We are considering the Mercury (Hg), confined in a Titanium tube duct, as a candidate for ILC target. One negative property of Mercury, what may strictly influence to the choice – is its toxicity. Hg considered as one of mostly toxic materials, it could be handled properly, however. In some installations the Mercury is in use in turbine circle, instead of water, what give assurance of success of its implementation for our purposes. Total amount of Mercury in circulation is about ~1-1.5 liters only and there will be not a problem to handle it. Let us mention here that Mercury target is under consideration for test at CERN[24] as a proton beam target for generation of muons. So the formalities can be resolved, if necessary.

Properties of Mercury represented in Table 1.

X_0	6.5, g/cm^2
l_{X0}	0.48, cm
Z	80
Density r	13.6, g/cm^3
Heat capacity, c_V	0.14 $J/g/^oK$ @ 1.96 $J/cm^3/^oK$
Melting temperature, T_{melt}	-38.87 ^{o}C
Boiling temperature, T_b	356.58 ^{o}C
Speed of sound v_s	1407m/s @293^{o}K
Grüneisen's coefficient $G(V)$	~2
Thermal conductivity	8.34 W/m/^{o}K
Latent Heat of vaporization C_L	294 J/g,
Electrical conductivity	1.04 10^6 1/ohm/m

Isotopes of Mercury are stable, except artificially created ^{194}Hg, which decays $^{194}Hg \rightarrow ^{194}Au$ with half lifetime ~444 years.

Let us take for estimations the average power deposition ~5 kW. So every second Q=5kJ is deposited in a target. The heating of target is done by electrons (Compton and from pairs) and by positrons. As the ratio of Compton cross section to pair creation (per g/cm^2) is

$$\frac{s_{Compton}}{s_{pair}} \cong \frac{1}{gZa} \sim 8.5\%,$$

[24] H.G. Kirk, et. al., "*A High Power Target Experiment*", PAC 2005, Knoxville, TN, Proceedings, p. 3785.

Compton electrons practically do not heat the target; indeed, positrons and electrons from pairs generated in equal quantities and, hence, heat the target equally. As the number of positrons/electrons linearly increases along the path in a material of target, the energy deposition also increased linearly. So at the entrance it is zero deposition and heating, at the exit it is maximal. Namely this fact one need take into account while designing the input/output sides of the liquid metal duct. All this energy comes from the primary gamma bunch, so the estimations done are valid. As the gamma bunch has the length $ct \cong 0.3mm$ the pass-time for the bunch comes to $t \cong 1ps$, so one can consider initial conditions for the problem of heat as given at t=0 in a form of linear function along the target. Ratio of speed of sound in the Mercury to the speed of light confirms this assumption about instant deposition of energy. So the boundaries of the gamma beam trace and the heat deposited volume are congruent to the accuracy defined by the layer having thickness ~ $v_s \times t = (v_s / c) \times ct \sim (v_s / c) \times 0.3 \sim 1.4 \times 10^{-6} cm$.

Let the Mercury jet have a velocity of ?=10*m/sec* and dimensions S=1×0.24 cm^2 in cross section. So the volume passed per second is $V \cong 240cm^3$. Due to turbulence all energy is deposited evenly. The temperature gain becomes

$$DT \sim \frac{Q}{rVc_V} \sim \frac{5000}{12.6 \times 240 \times 0.14} \sim 12^{\circ}\mathrm{C},$$

So from the point of average power deposition everything is acceptable.

Target unit is shown in Fig. 20. Here the Mercury at conversion point is running in the channel with rectangular cross-section in profiled Titanium duct. At the bottom of extension there is the Mercury surface as the flow is interrupted by profiled extension.

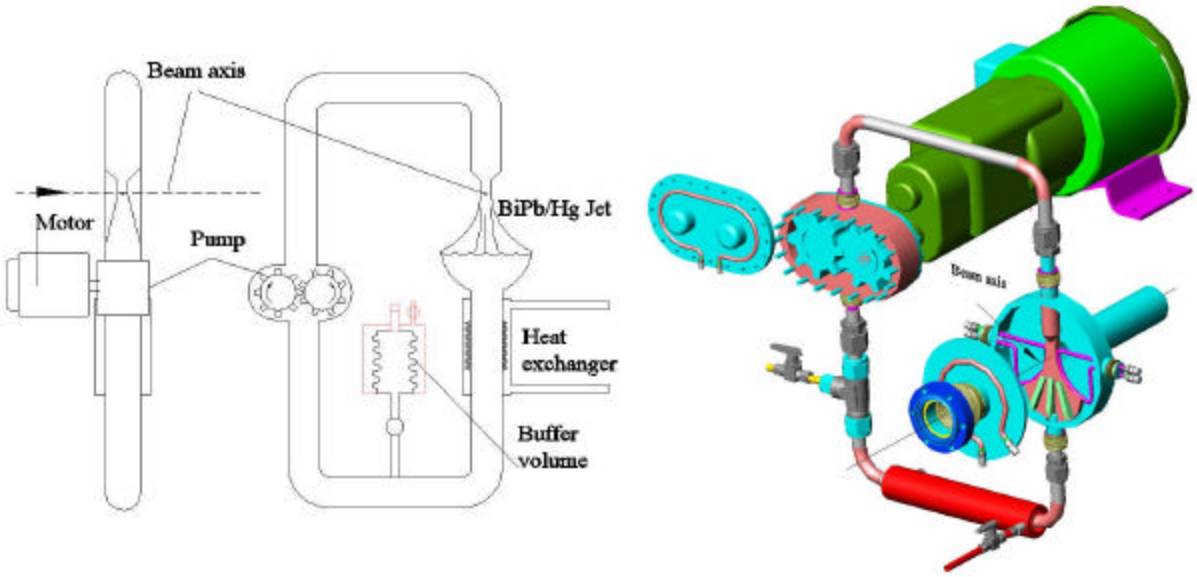

Figure 21: Scheme of liquid target, left. 3D view of the jet chamber is represented at the right. Diameter of the chamber is ~10 cm.

For $t \cong$ 300 nsec the jet will pass $L \cong vt = 10m/\sec \times 300 \cdot 10^{-9} = 3 \cdot 10^{-6} m = 3mm$ only, but for the time while the train passes, the distance will be $L \cong vt = 10m/\sec \times 10^{-3} = 10 \cdot 10^{-3} m = 1cm$. Energy deposited in the target *by one train* will be

$$Q_{train} = \frac{Q}{f} \cong \frac{5 \cdot 10^3}{5} \cong 1000 J$$

in a volume $V \cong LS \cong 1cm \times 1 \times 0.24 = 0.24 cm^3$, so for the temperature gain $\Delta T \cong 320^o C$ (starting from T=37^{0}C) the energy absorbed will be

$$Q \cong r V c_V \Delta T \cong 13.6 \times 0.24 \times 0.14 \times 320 = 146[J]$$

While becoming a vapor, the latent heat of vaporization needs to be applied to the liquid. Specific latent heat of vaporization for Mercury at 357 ^{o}C is C_L=294 *J/g*, so the energy absorbed by volume V=0.24cm^3 will be

$$Q_L \cong rVC_L \cong 13.6 \times 0.24 \times 294 = 959 J$$

So the total energy absorbed by this volume will be

$$Q_{tot} \cong 959+146=1105[J]$$

This number means that Mercury *will remain liquid* at boiling temperature, however. For the single bunch, one can estimate the energy deposition as

$$Q_{bunch} @ Q / n_b = 5000/2820 \ @ 0.18 \ J$$

The transverse size of gamma-beam at the target defined by angular divergence ant the distance L from undulator to the target, see (10)

$$s_{\wedge g} @ L \times \frac{\sqrt{1+K^2}}{g} \qquad (20)$$

Substitute here $L @ 150m = 1.5 \times 10^4 cm$, $g @ 3 \times 10^5$, $K^2 @ 0.15$ one can obtain,

$$s_{\wedge g} @ 1.5 \times 10^4 \times \frac{\sqrt{1.15}}{3 \times 10^5} @ 0.036 cm,$$

so the temperature of the volume $V @ p s_{\wedge g}^2 l_{X_o} / 2$ giving density of energy deposition $Q_{bunch} / rV \cong 14 \ J/g$ and the temperature gain at least

$$DT @ \frac{Q_{bunch}}{r \times p \, s_{\wedge g}^2 \, 0.24 \times c_V} @ \frac{0.18}{13.6 \times p \times 1.3 \times 10^{-3} 0.24 \times 0.14} @ 125^o.$$

The temperate distributed linearly from zero at the entrance of the jet to double of this at the exit. So for the single bunch the conditions are acceptable, what means that average values we took for the train are allowable here.

Thus the droplets condensed at the bottom metal surface. Looks like the mass depletion effect needs to be taken into account, however. The mixture of vapor and drops hit the mercury surface. The liquid surface accepts the shocks from droplets. So, this target is able to absorb ~5 kW under the parameters specified.

Remember, the speed of Mercury jet was taken 10 m/s only. For velocity of jet

$$v \cong \sqrt{P / r} \ ,$$

where P stands for pressure at the entrance of jet chamber. For moderate pressure P=30 *kg/cm^2* (30 atm), one can expect the velocity 21m/s. So that is the real resource here. We would like to

say, that the Mercury flow in other parts of the loop, outside the LMJC, is slow due to extended diameter of tubes.
So the basic conclusion here is that Mercury satisfies requirements. Its toxicity however can make its implementation and usage in converter more difficult, so the Bi-Pb alloy is the best candidate under this circumstance for conversion of gammas into positrons. Its moderate melting temperature (~125 ^{o}C) can be tolerated with LMJC described above. The boiling temperature of this last alloy is much higher, ~1500 ^{o}C , what makes utilization of latent heat practically impossible, so the temperature raise of liquid is higher and all defined by heat capacity of Bi-Pb alloy ($0.15 J/g/^{o}K$, $r_{Liquid} @ 10.57\ g/cm^3$). One additional advantage of B-_Pb Targetry is its low thermal neutron cross-section (0.11 *barn*, compare with 389 *barn* for Hg)

Accelerating structure right after the target and collection system more likely is a copper conducting one immersed in solenoidal field. Additional focusing can be arranged with the help of irises having elliptical passing holes. Orientation of axes of these ellipses at opposite sides of cavities turned with 90 degrees. The following structure(s) might be SC ones. However, as at the front of structure there is a collimator, the first structure also can be a SC one.

COLLIMATOR

Sectioned collimator for enhancement of polarization of undulator radiation and for protection of undulator introduced a time ago[18]. Idea of collimation appeared even earlier [8,25]. In this collimator, the first sections made on light material (Be), the following sections made from heavy material. In this example the Iron used as it can be magnetized in azimuthal direction to defocus the secondary particles from axis. I n this geometry the B~15-20 kG can be reached with a small axial current running in cylindrical Copper-made enclosure.

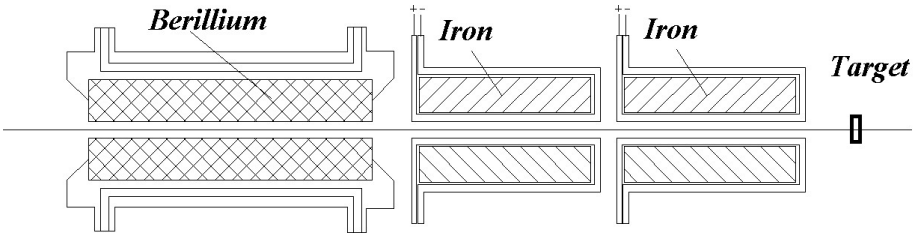

Figure 22: Sectioned collimator[18].

The primary electron beam with energy E_0, when hits the media, develops a cascade, what is a mixture of electrons, positrons and gammas. Namely these gammas are responsible for positron creation in electric field of nucleus of target material. This cascade develops along the target starting from the points of penetration of initial beam. The cascade propagates inside matter until energy of particles reaches the critical value, $E_c @ 610/(Z+1.24)$, MeV; Z stands for atomic number. Transverse size of the cascade in maximum is of the order of Molière radius $R_M @ X_0 E_s / E_c$, where X_0 is a radiation length,

[25] E.A.Bessonov, A.A. Mikhailichenko (Novosibirsk, IYF), *" Some aspects of undulator radiation forming for conversion system of the linear collider"*, BUDKER-INP-1992-43, Jun 1992. 26pp. http://ccdb4fs.kek.jp/cgi-bin/img/allpdf?199302032

$$X_0^{-1} \cong 4r_0^2 a \frac{N_A}{A} Z(Z+1)\ln\left(\frac{183}{Z^{1/3}}\right)[cm^2/g], \quad (21)$$

A –is atomic weight of target substance, $N_A \cong 6.022 \cdot 10^{23}$ is the Avohadro number, Z is atomic number, $a = e^2/\hbar c \approx 1/137$, r_0 is classic electron radius. $E_s = \sqrt{4\pi/a}\cdot mc^2 \cong 21.2 MeV$ –is a scale energy. Naturally, the Molière radius, expressed in cm, is bigger for lighter materials, as $R_M \approx 0.035 \times Z \times X_0$ and $X_0 \propto A/Z^2$, so $R_M \propto A/Z$, where A is atomic weight. For W with its Z=74, $R_M^W \approx 2.57 X_0$ ($l_M^W = 0.9$cm), as geometrical length corresponding to the radiation one is $l_{X_0} \approx 0.35 cm$. For Ti, with its Z=22, $R_M^{Ti} \approx 0.7 X_0$ ($l_M^{Ti} = 2.45$cm), as $l_{X_0} \approx 3.55 cm$. Cascade reaches its maximum at the depth $t_{max} \approx X_0 \ln(E_0/E_c)/\ln 2$ with the number of the particles there about $N_{max} \approx E_0/E_c$. So one can estimate geometrical volume occupied by cascade as

$$V_c \approx \frac{\pi}{3} l_{t_{max}} l_M^2 \approx \frac{\pi}{3\ln 2} l_{X_0}^3 \left(\frac{E_s}{E_c}\right)^2 \ln\frac{E_0}{E_c} \propto l_{X_0}^3 \times Z^2 \propto A^3/Z^4 .$$

The ratio of these volumes for Tungsten and for Titanium becomes $V_c^{Ti}/V_c^W \propto \left(\frac{l_{X_0}^{Ti}}{l_{X_0}^W}\right)^3 \times \left(\frac{Z^{Ti}}{Z^W}\right)^2 = \left(\frac{3.55}{0.35}\right)^3 \times \left(\frac{22}{74}\right)^2 \approx 88$, i.e. the volume involved in cascade inside Ti is about 88 times the volume inside W for the same initial energy of primary electrons. The number of particles in cascade for W will be ~3.4 times bigger than in Ti. Of course, this is estimation only, and gives qualitative numbers; accurate calculation needs to be carried numerically.

So depending on the task, the transverse size of collimator can reach couple Molière radiuses. We concentrate at the following collimator, Fig. 23.

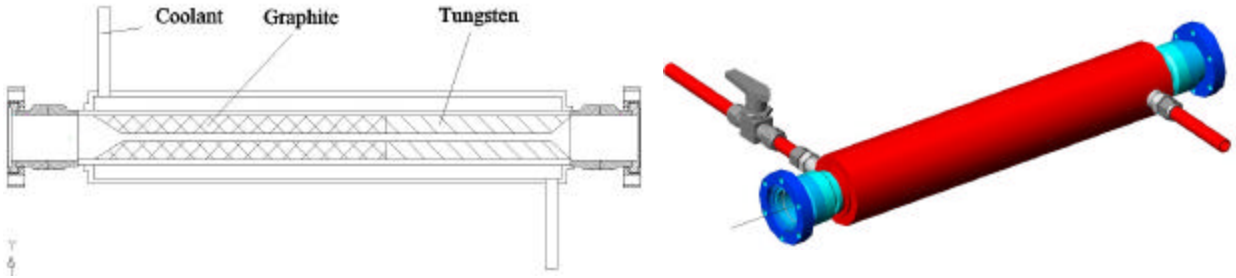

Figure 23: Collimator with Graphite. Flanges are 2 ¾ inch in diameter.

Pyrolytic Graphite (PG) is used here. The purpose of it is to increase the beam diameter, before entering to the W part. Vacuum outgassing is negligible for this material. Heat conductivity ~300 W/m-^{o}K is comparable with meals. Also, the Graphite is denser, than Be.

Another example is a *collimator with rotating liquid*[26]. Represented in Fig. 23 device is a contemporary design of this device.

[26] Similar type of collimator considered for VLEPP, [23].

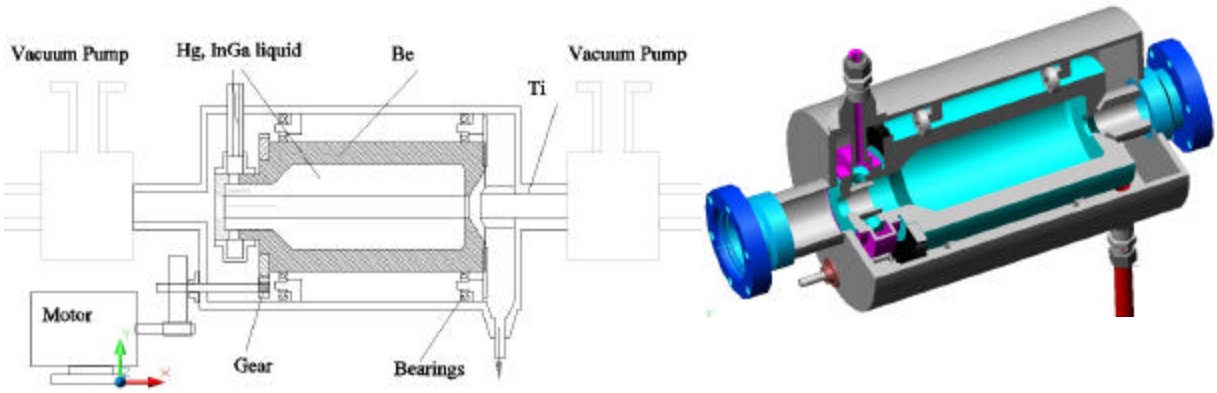

Figure 24: High average power collimator. Beam is coming from the right.

To fill the inner volume, the cylinder and liquid must have angular speed $w \geq \sqrt{g/r}$, where g=9.8m/s^2, and r stands for the inner radius. Let us take for estimations r =2mm=0.002 m, then $w \geq \sqrt{9800/2}$ =70 rad/s or 11 turns/s. The last number looks reasonable.
In the Figure 23, at the right side, the diameter of the hole in bottom of Be cylinder is smaller, than at the left side.

This collimator surrounded by pumping stations from both ends. These stations contain the Cold traps (cooled by Liquid Nitrogen) to avoid metal dispersion to the surrounding vacuum channels.

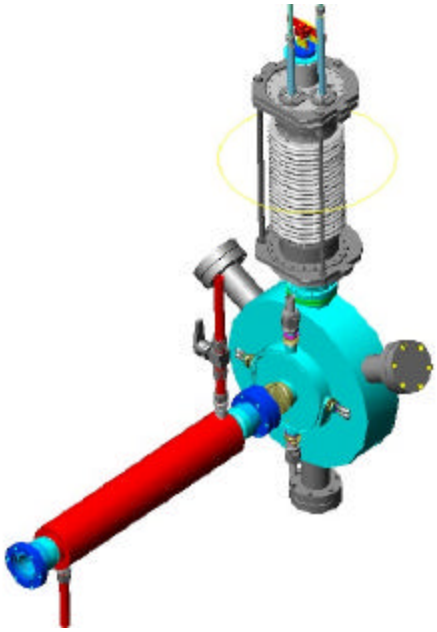

Figure 25: Conversion module assembled. Flange shown is a 2¾ inch. Elements of transverse motion of these devices for proper spatial positioning are not shown here.

MODELING OF SC UNDULATOR

As far as engineering issues, we have tested 30-cm long, 1 cm period undulator having aperture 6mm. New ones will be manufactured with improved tapering and winding.

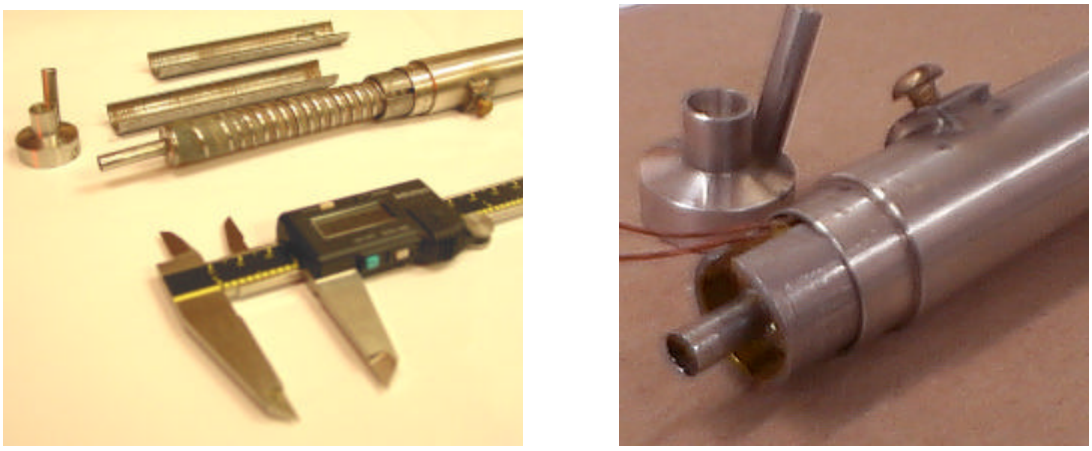

Figure 26: Undulator having a period of 10 mm and aperture 6mm develops $K \cong 0.33$ for I=200A. Tube diameter is 6 mm. Tested up to 400 A.

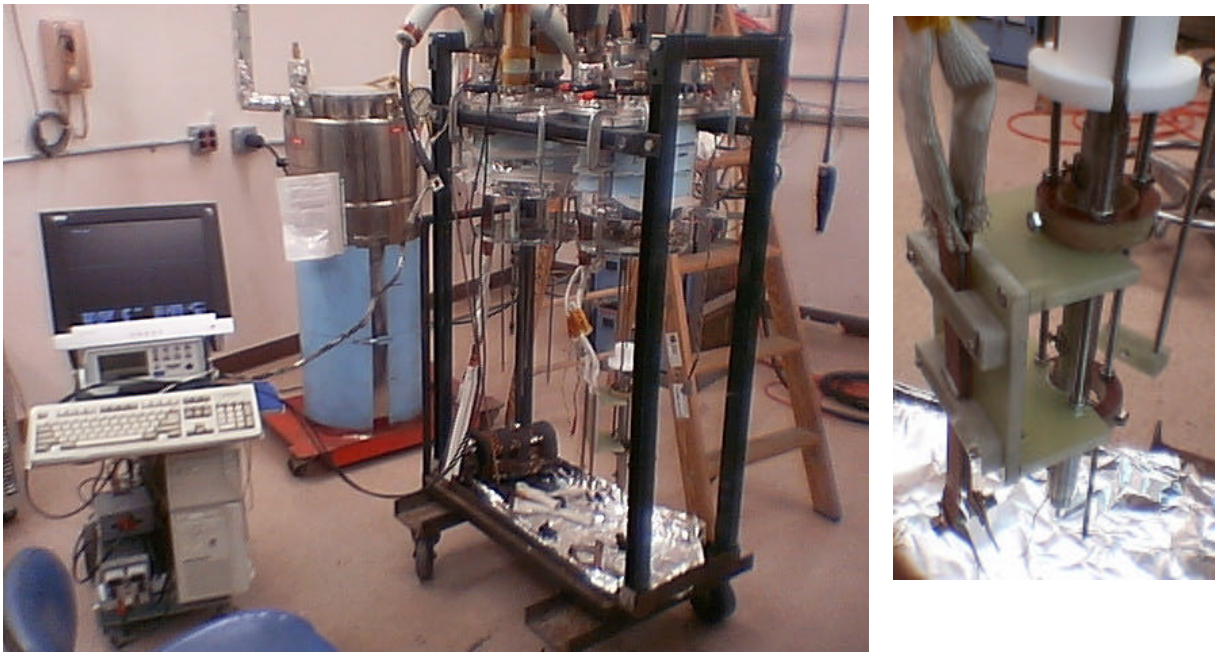

Figure 27: Cold mass test.

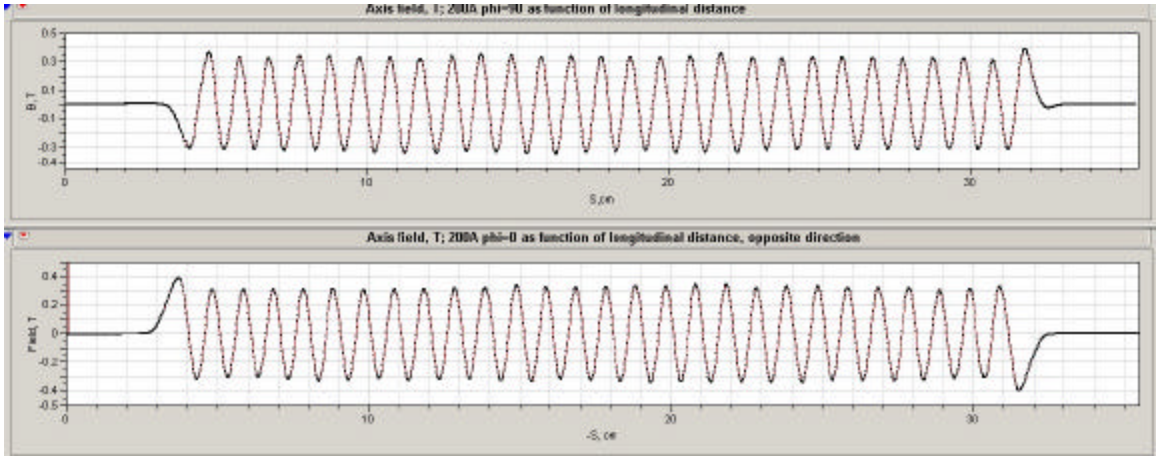

Figure 28: Longitudinal field profile measured with Hall probe at Cornell. K=0.33 as required.

CONCLUSIONS

Undulator scheme is preferable for positron production at all times. It is not important—polarized positrons required or not.

Cornell has experience in positron collection optics design. Recent innovations allow collection of 100 mA/ min in CESR ring (perimeter=768m). And this is after acceleration in synchrotron with its inevitable losses.

Fabrication of full scale 4 m—long module allows to test it with real beam and get real cost estimation. Each 4-m long module includes PS, movers, pickups, trim coils/lenses. About 50 modules required, coming to the cost ~$10M for all undulator.

Schemes for the target, collimator and focusing lens look feasible. Bi-Pb target looks like pretty well guarantied. Hg target looks feasible also. Design of liquid metal jet chamber allows accommodation any of these. Final cost estimation will be done after the first real scale prototype will be manufactured.

Our vision of post target hardware –RF, spin rotators will be considered is separate publication. For spin rotator we are considering single line scheme with fast reversible magnetic field.

This work supported by NSF.

APPENDIX

EMITTANCE PERTURBATIONS

Influence of the field roll-off in undulator

Inside undulator particles developing tiny helixes, having pitch angle $a \sim K/g$, and the radius of helixes is $a @ \lambda_u K/g$, where $\lambda_u = l_u/2p$, l_u stands for period of undulator; we will be interested in $l_u \cong 1\ cm$. The numbers for angular spread and radius of helix for E=150 GeV ($g @ 3 \times 10^5$), and K~1 coming to $a \sim 3 \times 10^{-6}$ rad and $a \cong 10^{-5}/6p \cong 5 \cdot 10^{-7} cm$ respectively.

Meanwhile natural vertical angular spread inside the beam and the beam size $y' \sim \sqrt{ge_z / b g}$ and $\sqrt{\langle y^2 \rangle} \cong \sqrt{ge_y b / g}$, for invariant vertical emittance $ge_z \sim 2 \times 10^{-8} m \times rad$ and the envelope function value $b \sim 100m$, go to be

$$y' \sim \sqrt{2 \times 10^{-8} / 3 \times 10^5 / 100} \sim 2.6 \times 10^{-8} \text{ rad and } \sqrt{\langle y^2 \rangle} \cong \sqrt{2 \cdot 10^{-8} \cdot 100 / 3 \cdot 10^5} \cong 2.6 \cdot 10^{-4} [cm]$$

respectively. For horizontal motion, $ge_x \cong 2 \cdot 10^{-6} m \cdot rad$ giving all numbers ten times bigger.

Angular spread in radiation	$a \sim \sqrt{1 + K^2} / g$	3×10^{-6} (K=1)
Angular spread in beam, vert.	$y' \sim \sqrt{ge_z / b g}$	2.6×10^{-8}
Radius of helix	$a \sim \lambda_u K / g$	$5 \times 10^{-7} cm$ (K=1)
Beam size, vertical	$\sqrt{\langle y^2 \rangle} \cong \sqrt{ge_y b / g}$	$2.6 \cdot 10^{-4} cm$
Beam size, radial	$\sqrt{\langle x^2 \rangle} \cong \sqrt{ge_x b / g}$	$2.6 \cdot 10^{-3} cm$

One can see that angular wiggling is much bigger, than natural angular spread in the beam. Meanwhile the radii of helixes are much smaller, than the beam size. First fact makes possible angular separation for reduction of contest of second harmonic and enhancing average polarization as it becomes reversed under angle $\sim 1/g$. *Important thing here is that the power falling on the target is reduced also by the same procedure (angular selection).*

All particles in cross-section are developing helixes with the same phase inside undulator, despite field dependence across aperture. The last generates ellipticity in helix. The field roll-off from the center of undulator, described in polar coordinates, is proportional to the square transverse radial displacement r

$$H_j(r, j, z) \cong H_0 \times \cos(j - j_0 - \frac{z}{\lambda_u}) \times \left[1 + \frac{1}{8} \left(\frac{r}{\lambda_u} \right)^2 + \frac{1}{768} \left(\frac{r}{\lambda_u} \right)^4 + \ldots \right], \qquad \text{(A1)}$$

where $H_0 \propto I / \lambda_u$ is the field at the axis, I stands for the current running in helix[27]. So in our case the second term for the particles at the distance $\sqrt{\langle x^2 \rangle} \cong 26 \cdot 10^{-4} cm$ goes to be

$$\frac{1}{8} \left(\frac{r}{\lambda_u} \right)^2 \cong \frac{\langle x^2 \rangle}{8 \lambda_u^2} \cong 3.3 \cdot 10^{-5}, \qquad \frac{\langle y^2 \rangle}{8 \lambda_u^2} \cong 3.3 \cdot 10^{-7}.$$

This means, that ellipticity is negligible, however. Important is that the difference in kicks obtained by the particles across the beam size will be different in the same proportion, if the helix is ended suddenly. As the field along the particle's trajectory oscillating, the nonlinear kicks are oscillating too. So resulting kick averaged along period will be different in accordance with formula, where for radius the value $r \cong \lambda_u K / g$ needs to be substituted now. In this case

[27] A. Mikhailichenko, CBN 02-10, Cornell, LEPP, 2002.

$$\frac{1}{8}\left(\frac{a}{\lambda_u}\right)^2 \cong \frac{K^2}{8g^2} \cong \frac{0.15}{8\cdot 9\cdot 10^{10}} \cong 2\cdot 10^{-13},$$

so the resulting angle after one period will be

$$\Delta x' \cong H_0 \times \frac{K^2}{8g^2}\frac{l_u}{(HR)} \cong 0.4[T]\times 2\cdot 10^{-13}\frac{1[cm]}{5\cdot 10^4[T\cdot cm]} \cong 0.16\times 10^{-17} rad\,.$$

where magnetic rigidity of particle at 150 GeV was substituted $(HR) = 5\cdot 10^4[T\cdot cm]$ and H_0=0.4 T. After all M=10^4 periods the angle goes to be $\Delta x' \cong 0.16\times 10^{-16} rad \times 10^4 \cong 1.6\cdot 10^{-13} rad$. This angle needs to be compared with angular spread in the beam $\sim 2.6\times 10^{-8}$.

Focusing in undulator can be evaluated as the following. The integral of gradient field due to passage over one period is

$$\int G ds \cong H_0 K / g\ .$$

So the focal distance of the whole undulator helix will be

$$F \cong \frac{(HR)}{M\int G ds} \cong \frac{(HR)}{MH_0 K} g \cong \frac{5\cdot 10^4}{10^4 0.4\times 0.4} 3\cdot 10^5[cm] = 10^7[cm]\,.$$

What important here is that the plane of magnetic field can be well controlled.

Focusing in the field of undulator

After passage a single pole at off-axis distance *y*, effective kick comes to be

$$y' \cong \frac{aHy}{2(HR)} \cong \frac{KHy}{2(HR)g}, \qquad \text{(A2)}$$

where (*HR*) stands for magnet rigidity, *H* is undulator magnetic field. So the focal distance for undulator having length *L* goes to be

$$F \cong \frac{y}{y'}\frac{l_u}{L} = \frac{2(HR)\,l_u g}{KHL} \cong \frac{l_u^2 g^2}{K^2 Lp}. \qquad \text{(A3)}$$

For 300 *GeV* beam $(HR) \cong 10^6 kG\cdot cm$, $g \cong 6\cdot 10^5$, $K \cong 1$, $L \cong 100\,m$, $l_u \cong 1cm$ focal distance goes to be $F \cong 10^7 cm$. So the angle obtained by side particle can be estimated as

$$x \cong \frac{\sqrt{g e_x b\ /g}}{F} \cong x' \cong \frac{2.6\cdot 10^{-3}}{10^7} \cong 2.6\cdot 10^{-10},$$

meanwhile the angular spread in radial direction is $x' \cong 2.6\cdot 10^{-6}$. So the effect of focusing is negligible. Also with reduction of envelope function by lenses installed between sections of undulator, these numbers can be improved.

Focusing by alternative sextupole field is much smaller as one can see from the formula for magnetic field.

For planar undulator there is no focusing in direction across the poles (typically horizontal direction) at all. For this the pole must be wide enough. Practically, the pole width must be ~3-4 times the vertical pole gap size for these purposes. This is, probably, the only simplification in comparison with helical undulator.

Emittance perturbation due to radiation in dispersive field of undulator

As that undulator field has dispersion, radiation of quanta may cause emittance growth. Equation describing this process is[28]

$$\frac{de_{x,y}}{dz} \cong \left(H_{x,y} + \frac{b_{x,y}}{g^2} \right) \overline{d(E_g / E)^2} \qquad \text{(A4)}$$

$H(z) = \frac{1}{b(z)} \left(h^2(z) + (bh' - \frac{1}{2} b'h)^2 \right)$, z—is a longitudinal coordinate here, $\overline{A}$ -means averaging over spectrum of radiation. Dispersion generated inside undulator is a periodic solution

$$h = \frac{K\lambda_u}{g} Sin\frac{z}{\lambda_u}, \quad h'(z) = \frac{K}{g} Cos\frac{z}{\lambda_u}, \qquad \text{(A5)}$$

so dispersion invariant becomes $H \cong bh'^2 = \frac{bK^2}{g^2} Cos^2 \frac{z}{\lambda_u}$.

$$\overline{\left(\frac{E_g}{E}\right)^2} = \int \left(\frac{E_g}{E}\right)^2 \frac{dN_g}{dE_g} dE_g = \left(\frac{\hbar w_{\max}}{E}\right)^2 \int x^2 \frac{dN_g}{dx} dx \,, \qquad \text{(A6)}$$

and variable $x = \frac{E_g}{E_{g\max}} = \frac{1+K^2}{1+K^2+g^2J^2}$ is the same as used in (1).

Using formulas for undulator radiation (2), (3) and taking into account that

$$\int_0^1 x^2(1 - 2x + 2x^2)dx = 7/30, \quad ,$$

one can obtain formula for emittance dilution as

$$De \approx \frac{\overline{b}}{2} \frac{K^4}{(1+K^2)^3} \left(\frac{r_0}{\lambda_u}\right)^2 \times 2pM \times \frac{7}{30}, \qquad \text{(A7)}$$

where $\overline{b}$ stands for average envelop function in undulator. So perturbation of emittance due to this effect is negligible.

So finalizing one can say that the beam size is so small, that the difference in transverse kicks across the beam is small and perturbation of emittance is small too. Even so, the back up solution was here: to work in positron wing with doubled frequency and use one pulse just for positron generation, not for further acceleration. Fortunately this is not required.

This however is the mostly important subject for concern while attempting installation of undulator before IP.

[28] Radiation damping is neglected.

PERTURBATION OF POLARIZATION

Perturbations due to dynamical motion in helical field

As one can see that particles experience helical motion with pitch angle mentioned above $a \sim K/g$. Then vector of spin rotates relatively to momentum with the angle which is g/g_0 (g_0 corresponds to ~440.65 MeV) times faster. Important thing here is that resulting angle is going to be

$$q_{spin} = \frac{K}{g} \cdot \frac{g}{g_0} = \frac{K}{g_0}, \tag{A8}$$

i.e. this angle for each particle does not depend on its energy. The last means, that resulting angle for *all* particles in the bunch, having slightly different energies, is the same. This means, in its turn, that there is no depolarization at all. Formal consideration of the spin behavior done [29] shows that this is not a problem. The only thing needs to be done – is just controlled proper orientation of spin before undulator, so that after undulator it is directed as needed. One needs to prepare the initial spin orientation taking into account spin rotation in undulator.

Spin flip in undulator

Positron or electron may flip its spin direction while radiating in magnetic field. As primary beam is the beam of polarized particles (in case if undulator installed before IP), one can think about possible depolarization here.

Let us examine formula for the probability of radiation transaction (spin flip) for the circular motion in magnetic field[30]

$$\frac{1}{t}[\sec^{-1}] = w_{flip} = \frac{5\sqrt{3}}{16}\frac{r_0^2}{a}\frac{w_0^3}{c^2}g^5\left(1 - \frac{2}{9}z_{\|}^2 - \frac{8\sqrt{3}}{15}\frac{e}{|e|}z_{\wedge}\right), \tag{A9}$$

where $z_{\|}$, $z_{\wedge}$ stand for longitudinal and transverse components respectively, $w_0 = eH/mcg$. Probability of radiation in undulator per second (which is responsible for radiation at all) can be written as

$$w_{rad} = \frac{I}{\hbar w_0 2g^2} = \frac{2}{3}\frac{e^4 H^2 g^2}{m^2 c^3}\frac{1}{\hbar w_0 2g^2} = \frac{1}{3}a g^2 w_0 , \tag{A10}$$

so the ratio of these probabilities becomes

$$\frac{w_{flip}}{w_{rad}} = \frac{15\sqrt{3}}{16}\frac{\lambda\!\!\!^{-2}_c}{\lambda\!\!\!^{-2}_u}g^3\left(1 - \frac{2}{9}z_{\|}^2 - \frac{8\sqrt{3}}{15}\frac{e}{|e|}z_{\wedge}\right), \tag{A11}$$

---

[29] E.A. Perevedentsev, V.I. Ptitsin, Yu.M. Shatunov, *"Spin behavior in Helical Undulator"*. In *Hamburg 1992, Proceedings of 15th Int. Conf. on High-energy accelerators, vol. 1* 170-172. (Int. J. Mod. Phys. A, Proc. Suppl. 2A (1993) 170-172).

[30] Baier V., Katkov V., Fadin V., *"Electromagnetic Processes at High Energy in Oriented Crystals"*, World Scientific, Singapore, 1998.

where $\lambda\!\!\!^{-}_c = r_0 / a = e^2 / mc^2 / a \approx 3.8616 \times 10^{-11} cm$ is Compton wavelength, and here was substituted $\lambda\!\!\!^{-}_u = w_0 / c$ - normalized to $2p$ undulator wavelength. The last formula reflects the fact, that the particle radiated a lot of photons and influence to polarization is small.

Strictly speaking formula (A9) represented here is valid for circular motion in a strong magnetic field (big K factor), where characteristic energy of photon is $\hbar w_c \gg \hbar w_0 g^3$, i.e. even higher, than used for undulator radiation in (A10). So for simple circular motion this ratio is even less, than represented in (A11) by factor g

$$\frac{w_{flip}}{w_{rad}} \sim \frac{\lambda\!\!\!^{-2}_C}{\lambda\!\!\!^{-2}_u} g^2 .$$

It is interesting, that third term in brackets in formula (A11) describes the self polarization ratio to the damping time. So for parameters of our interest, where $g \approx 3 \times 10^5$, the effect of spin flip still small (i.e. radiation is dominating).

Perturbations due to radiation in a target

Similarly to the spin flip of polarized particles in undulator the spin might flip due to radiation of bremstrahlung quantas having energy $0 < \hbar w_g \leq E_1$, where E_1 stands for initial energy of positron. Depolarization after one single act of scattering defined as

$$D = 1 - \left| \frac{ds_{ge}(z_1, z_1) - ds_{ge}(z_1, -z_1)}{ds_{ge}} \right|, \qquad \text{(A12)}$$

where $ds_{ge}(z_1, z_1)$ stands for bremstrahlung cross section without spin flip, $ds_{ge}(z_1, -z_1)$–the cross section with spin flip and ds_{ge} is total cross section. Substitute here formulas for each of these sections one can obtain[12]

$$D = \frac{\hbar^2 w_g^2 \times [1 - \frac{1}{3} z_1^2]}{E_1^2 + E_2^2 - \frac{2}{3} E_1 E_2}, \qquad \text{(A13)}$$

E_2 stands for final energy of positron. As we are interesting in energetic secondary positrons, $\hbar w_g / E_1 << 1$ and $D = \frac{\hbar^2 w_g^2 \times [1 - \frac{1}{3} z_1^2]}{E_1^2} \approx 0$. Although depolarization after single collision is small, one needs to calculated resulting depolarization after passage some distance. This defines the length of depolarization associated with spin-flip while multiply scattering on nuclei[12]

$$L_{dep} \sim \frac{1}{n \int D(\vec{p}_1, z_1) ds} = \frac{1}{2 n s_{flip}} \qquad \text{(A14)}$$

Substitute here formula for cross section with spin flip, one can obtain after[12] that

$$L_{dep} \approx \frac{2X_0}{1-\frac{1}{3}z^2} \approx 3X_0, \tag{A15}$$

where X_0 stands for radiation length, (6). Optimal thickness of target is ~ ½ X_0. As probability of positron creation is linearly growing with passage distance for gamma quanta inside the target, effective thickness is going to be ~1/6 X_0, so resulting depolarization is going to be $D \approx \exp(-1/18) \approx 1-1/18 \approx 5\%$. So this effect is small and generally speaking is not associated with the choice of undulator – this is general effect.

Kinematical perturbations due to multiple scattering in a target

Let us consider the possible effect of *kinematical* depolarization associated with rotation of spin vector while particle experience multiple scattering in media of target before leaving. Typically polarized positron carries out ~(0.5-1) $\hbar\omega$ –energy of gamma quanta. As positrons/electrons created have longitudinal polarization, it is good to have assurance that during scattering in material of target polarization is not lost. Each act of scattering is Coulomb scattering in field of nuclei. So BMT equation describing the spin $\vec{z}$ motion in electrical field of nuclei looks like

$$\frac{d\vec{z}}{dt} = \frac{e}{mc^2\gamma}\left[G\gamma + \frac{\gamma}{\gamma+1}\right]\vec{z}\times\left(\vec{E}\times\vec{v}\right), \tag{A16}$$

where $\vec{E} \sim Ze\vec{r}/r^3$ stands for repulsive (for positrons) electrical field of nuclei, factor $G = \frac{g-2}{2} \approx 1.1596\times10^{-3} \approx \frac{a}{2\pi}$. Deviation of momentum is simply $d\vec{p}/dt = e\vec{E}$.

So the spin equation becomes

$$\frac{d\vec{z}}{dt} = \frac{1}{mc^2\gamma}\left[G\gamma + \frac{\gamma}{\gamma+1}\right]\vec{z}\times\left(\frac{d\vec{p}}{dt}\times\vec{v}\right). \tag{A17}$$

We neglected variation of energy of particle during the act of scattering, so $\frac{d\vec{p}}{dt} \approx m\gamma\frac{d\vec{v}}{dt}$ and vector $\vec{p}$ just changes its direction. Introducing normalized velocity as usual $\vec{b} = \vec{v}/c$, equation of spin motion finally comes to the following

$$\frac{d\vec{z}}{dt} = \left[G\gamma + \frac{\gamma}{\gamma+1}\right]\vec{z}\times(\dot{\vec{b}}\times\vec{b}) = \left[G\gamma + \frac{\gamma}{\gamma+1}\right]\vec{z}\times\frac{d\vec{j}}{dt}, \tag{A18}$$

where j stands for the scattering angle and the vector $d\vec{j}/dt$ directed normally to the scattering plane. For intermediate energy of our interest $\gamma \sim 40$, so the term in bracket ~1 and, finally

$$\frac{d\vec{z}}{dt} \approx \vec{z}\times\frac{d\vec{j}}{dt}. \tag{A19}$$

The last equation means that spin rotates to the same angle as the scattering one, i.e. spin follows the particle trajectory.

Depolarization at IP

Depolarization arises as the spin changes its direction in coherent magnetic field of incoming beam. Again, here the deviation does not depend on energy, however it depends on location of particle in the bunch: central particles are not perturbed at all. Absolute value of angular rotation has opposite sign for particles symmetrically located around collision axes.

This topic was investigated immediately after the scheme for polarized positron production was invented. This effect is not associated with polarized positron production exclusively because this effect tolerates to the polarization of electrons at IP as well. Later many authors also considered this topic in detail. General conclusion here is that depolarization remains at the level ~5%[31].

[31] E.A. Kushnirenko, A. A. Likhoded, M.V. Shevlyagin, *"Depolarization Effects for Collisions of Polarized* e^+e^- *beams"*, IHEP 93-131, SW 9430, Protvino 1993.